Journal of Rock Mechanics and Geotechnical Engineering 14 (2022) 637–652

Contents lists available at ScienceDirect

Journal of Rock Mechanics and Geotechnical Engineering

journal homepage: www.jrmge.cn

Full Length Article

Evaluation of hydro-mechano-chemical behaviour of bentonite-sand mixtures

Wenjing Sun [a,b,c,*], Cheng Liu [d,e], Diansen Yang [c], Dean Sun [e]

[a] Department of Civil and Energy Engineering, College of Environmental Science and Engineering, Donghua University, Shanghai, 201620, China
[b] Institute for the Conservation of Cultural Heritage, Shanghai University, Shanghai, 200444, China
[c] State Key Laboratory of Geomechanics and Geotechnical Engineering, Institute of Rock and Soil Mechanics, Chinese Academy of Sciences, Wuhan, 430071, China
[d] Shanghai Construction Group Co., Ltd., Shanghai, 200080, China
[e] Department of Civil Engineering, School of Mechanics and Engineering Science, Shanghai University, Shanghai, 200444, China

ARTICLE INFO

Article history:
Received 10 February 2021
Received in revised form
31 July 2021
Accepted 18 October 2021
Available online 20 December 2021

Keywords:
Bentonite-sand mixture
Hydro-mechano-chemical (HMC) behaviour
Salt solution
True effective stress

ABSTRACT

Bentonite-sand mixtures are widely used in engineering barrier of deep geological disposal of high-level radioactive nuclear waste and anti-seepage barrier of civil geotechnical engineering. Under the action of groundwater solution infiltration and external stress, the hydro-mechanical (HM) behaviour of bentonite-sand mixtures, i.e. the swelling characteristics and permeability, will change. Once the anti-seepage and filtration effect is weakened or lost, the pollutants will spread to the biosphere. Therefore, it is necessary to study the swelling characteristics and permeability of bentonite-sand mixtures under coupled mechano-chemical (MC) effect and to establish corresponding prediction model. For this reason, swelling tests under salt solution with different concentrations are conducted on pure bentonite and its mixtures with 30%, 70% and 90% sand contents, the compression tests are carried out on saturated samples, and the saturated permeability coefficient k of the sample under each load is calculated by Terzaghi's one-dimensional consolidation theory. The concepts of true effective stress p_e, montmorillonite void ratio e_m and critical sand content α_s are introduced to determine the e_m-p_e relationship and finally the k-e_m relationship of bentonite-sand mixtures. It is found that when the sand content $\alpha \leq \alpha_s$, the e_m-p_e relationship of the mixture is linear and independent of the salt solution concentration, and when $\alpha > \alpha_s$, the e_m-p_e relationship of bentonite-sand mixture is bi-linear with the true effective deviatoric stress $p_{es\alpha}$ as the intersection. In addition, the e_m-k relationship also shows the linear trend when $\alpha \leq \alpha_s$, and the slope of the line increases with the increase of the salt solution concentration. When $\alpha > \alpha_s$, the k-e_m relationship will deviate from the linear relationship. Moreover, the larger the sand content is, the farther the deviation is. On the basis of summing the regularity, a model for predicting the HM behaviour of bentonite-sand mixture under the coupled MC effect is proposed. By comparing the swelling and permeability test results with model prediction results of different types of bentonite and its sand mixtures, the predictive model is verified. The study on the HM behaviour of bentonite-sand mixtures under salt solution infiltration and the model establishment can provide experimental and theoretical basis for the design and construction of anti-seepage engineering by bentonite-sand mixtures.

1. Introduction

Bentonite is an ideal material in the artificial engineering barrier for deep geological disposal of high-level radioactive nuclear waste (HLW), landfills and cultural relic protection, due to its high expansibility, low permeability and excellent adsorption capacity (Ye et al., 2010; Shackelford et al., 2010). As the engineering barrier in HLW repository, different countries suggested different mixing ratios between bentonite and sand for buffer/backfill materials, considering the anti-seepage performance, storage capacity and economic benefits. For example, Sweden adopted pure bentonite (SKB, 2010); China adopted pure Gaomiaozi bentonite (Wang, 2010; Wang et al., 2018); Canada recommended 50% bentonite and 50% sand as buffer/backfill material (AECL, 1994); Czech Republic used mixture of Rokle calcium-based bentonite, sand and graphite with a dry mass ratio of 85:10:5

* Corresponding author. Department of Civil and Energy Engineering, College of Environmental Science and Engineering, Donghua University, Shanghai, 201620, China.
E-mail address: wjsun@dhu.edu.cn (W. Sun).

Peer review under responsibility of Institute of Rock and Soil Mechanics, Chinese Academy of Sciences.

https://doi.org/10.1016/j.jrmge.2021.10.008

(Pacovsky et al., 2007); and Japan planned to use mixture of 70% bentonite and 30% sand as the buffer material and 30% bentonite and 70% sand as the backfill material (JNC, 1999). In anti-seepage barriers in geotechnical engineering structures, such as landfills, the horizontal impervious layer is usually composed of pure bentonite and the vertical cutoff wall adopts bentonite enhanced materials (Evans et al., 2008; Fan et al., 2014), about 4%–12% bentonite content, which can meet the US Environmental Protection Agency (EPA) regulations on the permeability (Alawaji, 1999).

vCompared to pure bentonite, bentonite-sand mixtures have the higher strength and thermal conductivity. However, the mixture shows the lower swelling characteristics, which affects its sealing performance (Mollins et al., 1996; Karnland et al., 2008). At the same time, the swelling characteristics and permeability of the mixture will be influenced by the other factors, such as temperature (Shirazi et al., 2010; Cui et al., 2018), sand grain size (Sivapullaiah et al., 2000; Shirazi et al., 2010; Monkul and Yamamuro, 2011; Cabalar and Hasan, 2013; Srikanth and Mishra, 2016; Wang et al., 2021), and the salt in groundwater (Komine et al., 2009; Sun et al., 2015a). It is indicated that the salt content in the groundwater near the coastal nuclear waste repository and landfill site is higher (Komine et al., 2009; Fan et al., 2014). Moreover, the groundwater in inland regions is also very salty due to transpiration. China's nuclear waste geological repository is located in Beishan, Gansu Province (Wang, 2010; Wang et al., 2018), where the groundwater salt concentration is relatively high (Sun et al., 2015a).

Under external stress and the infiltration of groundwater, the hydro-mechanical (HM) behaviour, i.e. the swelling characteristics and permeability of bentonite-sand mixture, will change, which are the important basis for evaluating the long-term anti-seepage performance of engineering barriers. Once its anti-seepage and filtration capacity is weakened or lost, the pollutants will accelerate the spread to the biosphere. Therefore, it is necessary to study the swelling characteristics and saturated permeability of bentonite-sand mixture under coupled mechano-chemical (MC) effect.

In addition, due to extremely low permeability of bentonite, it takes a long time to determine the swelling characteristics and permeability of bentonite-sand mixture through experiments, and many factors such as mixing ratio, salt type and concentration of groundwater must be considered. Therefore, in order to meet the needs the requirements of design and evaluation of impervious barrier for bentonite-sand mixtures, it is urgent to propose a model for predicting the HM behaviour of bentonite-sand mixtures under coupled MC effect.

At present, many scholars have studied the swelling characteristics and permeability of different types of bentonite and its sand mixtures, for example, FEBEX bentonite (Villar and Lloret, 2008), Kunigel V_1 sodium bentonite (Komine and Ogata, 1994; Komine, 2004; Sun et al., 2009), Calcigel calcium bentonite (Agus and Schanz, 2008), MX80 bentonite (Wang et al., 2012), and Gaomiaozi sodium bentonite (Ye et al., 2010; Sun et al., 2013). The above swelling and permeability experiments were carried out with distilled or deionized water to avoid ion exchange between the solution and bentonite. However, when infiltrated by salt solution, the physico-chemical properties of bentonite are different with those under distilled or deionized water, leading to the changes in swelling and anti-seepage capacities (Zhang et al., 2012a; Zhu et al., 2013). The weakening effect of chemical composition in solution on swelling potential of bentonite is related to the chemical environment of the solution, the properties of bentonite, the external stress conditions, etc. (Alawaji, 1999; Castellanos et al., 2008; Herbert et al., 2008; Komine et al., 2009). Moreover, the main factors affecting the permeability coefficient of bentonite include the aggregate size, the montmorillonite content, the adsorption layer thickness, the hydration conditions, the void ratio, the type and concentration of the solution, the dielectric dispersion of soils, etc. (Petrov et al., 1997; Thevanayagam and Nesarajah, 1998; Komine et al., 2009).

In terms of swelling prediction model, the montmorillonite swelling volumetric strain (Komine and Ogata, 2004), the montmorillonite void ratio (Sun et al., 2009; 2015b, 2017), and the effective clay density (Zhang et al., 2012b) were adopted in the swelling prediction of bentonite-sand mixtures. The above prediction methods did not consider the effect of salt solution on swelling. Sun et al. (2015a) proposed swelling prediction model of bentonite saturated by different total dissolved solid (TDS) solutions using the montmorillonite void ratio. In terms of permeability prediction model, Sällfors and Öberg-Högsta (2002) and Komine (2008) predicted the permeability of bentonite-sand mixture with different sand contents, without considering the effect of salt solution. Katsumi et al. (2008) established the relationship between the free expansion rate and the saturated permeability coefficient of pure bentonite at lower dry density saturated under salt solutions with different concentrations and types. Tripathi (2013) predicted the permeability coefficients of different types of bentonite and its sand mixtures under the action of salt solution. A model proposed by Guimaraes et al. (2013) can simulate the saturated permeability of bentonite under different MC loading paths, based on the existing double-layer structure model, and considering the effects of ion content and cation exchange on the microstructure of expansive soils.

The above models predicted the swelling characteristics and permeability respectively. However, the permeability of bentonite-inclusive mixture is connected with its swelling characteristics, i.e. the saturated permeability coefficient is related to the soil deformation, which is caused by the external stress. Therefore, the relationship among external stress, deformation and permeability coefficient is closely related. A model should be established to predict the swelling and saturated permeability of bentonite-sand mixture under pure water or salt solution infiltration.

Therefore, we need to establish a model on the basis of the swelling and permeability characteristics of bentonite-sand mixtures with different sand contents under the action of salt solution, which can comprehensively reflect the hydro-mechano-chemical (HMC) behaviour of bentonite-sand mixtures.

In this paper, the swelling tests on pure bentonite and its sand mixtures with 30%, 70% and 90% sand contents under salt solutions with different concentrations are conducted, and then the compression tests on saturated samples are carried out. The saturated permeability coefficient k at each load is calculated by Terzaghi's one-dimensional (1D) consolidation theory. Then, the e_m-p_e relationship and the e_m-k relationship of bentonite-sand mixtures are determined by introducing the concepts of true effective stress p_e, montmorillonite void ratio e_m and critical sand content α_s, and the deformation characteristics and saturated permeability of bentonite-sand mixtures under salt solution infiltration are obtained. Finally, a model for predicting the HM behaviour of bentonite-sand mixtures under coupled MC effect is proposed and verified. Through the model, once given the values of the external stress and the salt solution concentration, the deformation and saturated permeability coefficient of bentonite-sand mixtures can be deduced. Meanwhile, the type of bentonite and the sand content can also be determined according to the environmental salt concentration, the vertical stress and the anti-seepage requirements allowed by local regulations.

2. Tests and results

2.1. Materials and testing method

Sodium modified calcium bentonite in geosynthetic clay liner (GCL) bentonite and Fujian standard sand were used for tests.

Table 1
Mineral composition of GCL bentonite.

Component	Content (%)
Montmorillonite	45.8
Clinoptilolite	22.8
Feldspar	18.6
Calcite	4.4
Quartz	4.1

Table 2
Geotechnical properties of GCL bentonite and Fujian standard sand.

Material	Property	Value
Bentonite	Specific gravity, G_{sb}	2.71
	Liquid limit, w_L (%)	153.4
	Plastic limit, w_p (%)	26.8
	Plastic index, I_P (%)	126.6
	Swelling index, δ_s (mL/(2 g))	25
	Cation exchange capacity (cmol/kg)	50.7
Fujian standard sand	Specific gravity, G_{ss}	2.65
	Maximum dry density, ρ_{dmax} (g/cm^3)	1.98
	Minimum dry density, ρ_{dmin} (g/cm^3)	1.35
	Average particle size, D_{50} (mm)	0.34
	Non-uniform coefficient, C_u	1.97
	Compression index, C_c	0.08

Table 1 shows the main mineral compositions of bentonite, determined by X-ray diffraction analyses. The main mineral component of the bentonite is montmorillonite with content of 45.8%, and associated minerals are some clinoptilolite, feldspar, calcite, quartz, etc. The geotechnical properties of GCL bentonite and Fujian standard sand are presented in Table 2.

Bentonite and sand were mixed by weight ratio of 10:90, 30:70, 70:30 and 100:0, respectively. As previously mentioned, bentonite-sand mixture with different sand contents is used as buffer/backfill material or anti-seepage barrier in practical engineering. Therefore, bentonite-sand mixtures with 10% (Alawaji, 1999), 30% and 70% (JNC, 1999) bentonite content and pure bentonite (Wang, 2010) were selected. The ratio range is wide coverage to determine the HMC behaviour of bentonite-sand mixtures.

The compressed samples with the dry density of 1.5 g/cm^3 and the initial water content of 15% were prepared. The test apparatus and the prepared samples are presented in Fig. 1, where Fig. 1a shows the photo of oedometer; Fig. 1b shows the sampling device, i.e. the mixed soil specimens are placed in a sampler and compacted with a jack to prepare compacted samples with a diameter of 6.18 cm and a height of 2 cm; and Fig. 1c shows the four representative samples of bentonite-sand mixtures with sand content α of 0%, 30%, 70% and 90% in sequence. NaCl solution with different concentrations was prepared at 0 mol/L, 0.1 mol/L, 0.5 mol/L and 1 mol/L, using NaCl (analytical reagent) and deionized water in the tests.

In engineering practice, the swelling of bentonite-sand mixtures can be considered as a 1D expansion or swell under constant stress. Gens and Alonso (1992) put forward three common swelling test methods: constant volume loading, loading after wetting, and swelling under load. Among them, the second swelling test method-loading after wetting was adopted more often (Komine et al., 2009; Sun et al., 2009, 2015a; Shirazi et al., 2010; Ye et al., 2014). Moreover, the second method can not only obtain the swelling characteristics, but also determine the permeability according to the indirect method derived from consolidation theory. Therefore, the second swelling test method was used.

First, under the vertical stress of 25 kPa, the swelling deformation tests on the mixtures saturated by the NaCl solutions with different concentrations were carried out. After the completion of swelling deformation test, a series of compression tests on saturated samples was conducted in accordance with ASTM D2435/D2435M-11 (1995). From the above tests, the swelling deformation under constant vertical stress and compression curves of bentonite-sand mixtures with different sand contents can be obtained.

Sun et al. (2015b) presented that there is a state curve between the final void ratio and the vertical stress after full saturation for bentonite-sand mixtures with a specified sand content, and verified by different types of bentonite that the final saturated state of bentonite-sand mixture all fell on the final saturated $\log_{10}e$-$\log_{10}\sigma_v$ relationship under any vertical pressure. Therefore, no matter how large the stress is, or in other words, if the stress changes, not under 25 kPa, the final e-σ_v relationship after full wetting will still fall on the specific state curve.

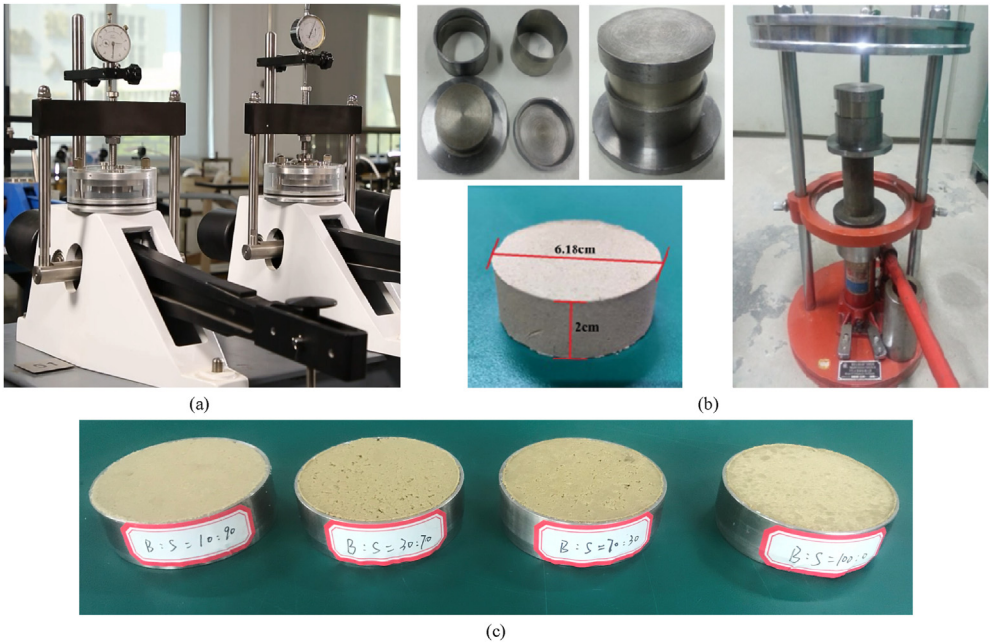

Fig. 1. Test apparatus and prepared samples: (a) Oedometer; (b) Sampling device; and (c) Bentonite-sand mixed samples with α = 0%, 30%, 70% and 90%.

Table 3
Plans for swelling and compression test.

No.	α (%)	m (mol/L)	ρ_{d0} (g/cm^3)	w_0 (%)	e_0	e_f	Loading path
1	0	0	1.5	15	0.947	1.567	Swelling tests under
2	0	0.1	1.5	15	0.939	1.497	25 kPa; Compression
3	0	0.5	1.5	15	0.942	1.385	tests under 25 kPa,
4	0	1	1.5	15	0.941	1.337	50 kPa, 100 kPa,
5	30	0	1.5	15	0.93	1.204	200 kPa, 300 kPa,
6	30	0.1	1.5	15	0.921	1.152	400 kPa, 600 kPa,
7	30	0.5	1.5	15	0.919	1.148	800 kPa, 1200 kPa
8	30	1	1.5	15	0.918	1.091	and 1600 kPa
9	70	0	1.5	15	0.787	0.714	
10	70	0.1	1.5	15	0.78	0.779	
11	70	0.5	1.5	15	0.783	0.788	
12	70	1	1.5	15	0.791	0.771	
13	90	0	1.5	15	0.788	0.748	
14	90	0.1	1.5	15	0.781	0.696	
15	90	0.5	1.5	15	0.789	0.743	
16	90	1	1.5	15	0.79	0.74	

Because of the low permeability of bentonite, it is difficult to measure the saturated permeability coefficient by conventional variable head permeability test method. Therefore, the saturated permeability coefficient was calculated using the indirect method derived from Terzaghi's 1D consolidation theory. Shirazi et al. (2010) performed a series of laboratory experiment on saturated bentonite-sand mixture prepared by distilled water, to investigate the permeability coefficient using direct permeability test by falling head method and indirect test methods derived from the consolidation theory. Sun et al. (2014) conducted a series of compression tests on saturated bentonite prepared by deionized water, and obtained the calculated saturated permeability coefficient using the indirect method derived from Terzaghi's 1D consolidation theory.

In this indirect method, the time, t_{90}, corresponding to 90% primary consolidation, was firstly estimated from the time-deformation curve from square root of time method (ASTM D2435/D2435M-11, 1995), i.e. the deformation readings, d, versus the square root of time (normally in minutes) for each increment of load. Then, the vertical consolidation coefficient c_v under each load was calculated through the formula: $c_v = 0.848\,\overline{h}^2/t_{90}$, where c_v is the vertical consolidation coefficient (cm^2/s), $\overline{h}$ is the average drainage path length and equal to half the average of initial height and final height at one vertical stress (cm). Finally, the saturated permeability coefficient can be calculated according to Terzaghi's 1D consolidation theory, i.e. $k = c_v m_v \gamma_w$, where k is the permeability coefficient (cm/s); m_v is the coefficient of volume compressibility (m^2/kN); γ_w is the unit weight of water, and $\gamma_w = 9.8$ kN/m^3. Subsequently, the permeability characteristics of saturated bentonite-sand mixture can be obtained.

Table 3 shows the test plans, including sand content α, salt solution concentration m, samples' initial state (initial dry density ρ_{d0}, water content w_0 and void ratio e_0), final void ratio e_f, vertical stress σ_v during water uptake, and loading paths in the compression tests.

2.2. Test results

2.2.1. Deformation of bentonite-sand mixtures infiltrated by salt solution

Fig. 2 shows the swelling deformation of pure bentonite and bentonite-sand mixtures with 30%, 70% and 90% sand contents

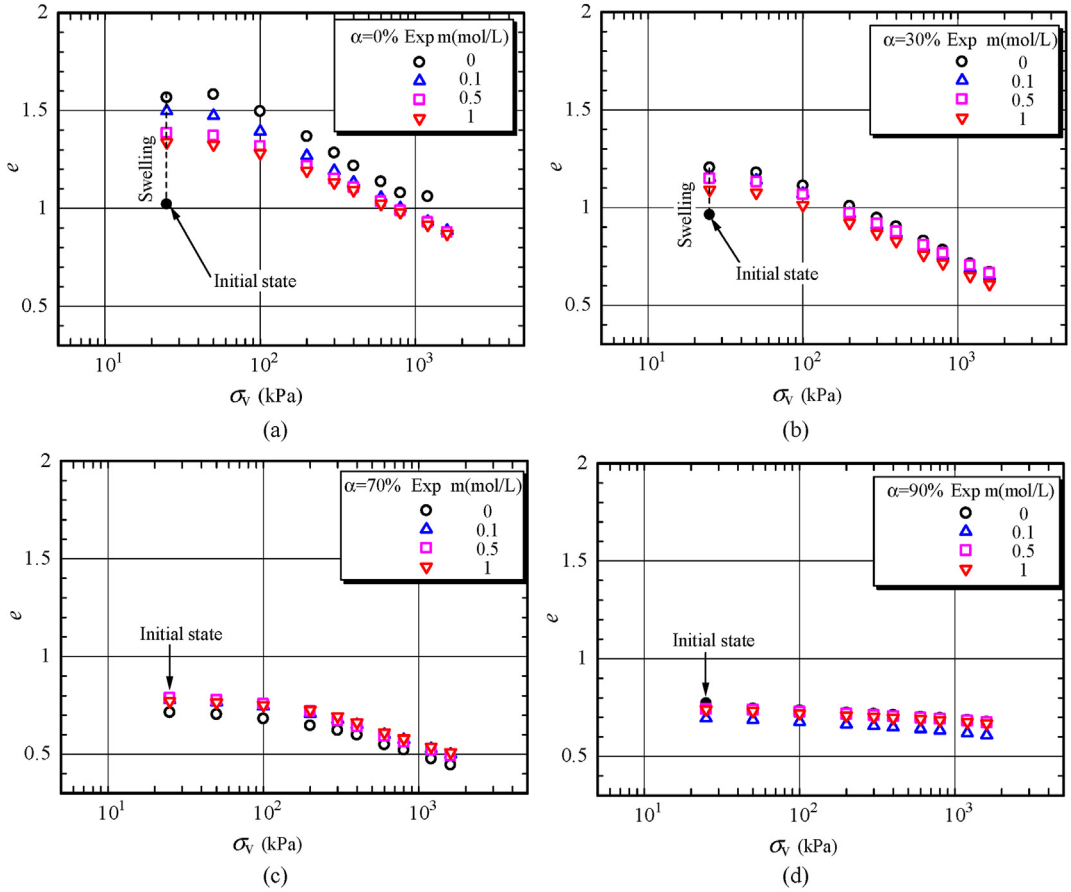

Fig. 2. Swelling and compression test results of bentonite-sand mixture infiltrated by salt solution: (a) α = 0%, (b) α = 30%, (c) α = 70%, and (d) α = 90%. Exp stands for the experiment.

Table 4
Compression data of bentonite-sand mixtures after full swelling.

No.	α (%)	m (mol/L)	ρ_{d0} (g/cm^3)	w_0 (%)	e									
					σ_v = 25 kPa	σ_v = 50 kPa	σ_v = 100 kPa	σ_v = 200 kPa	σ_v = 300 kPa	σ_v = 400 kPa	σ_v = 600 kPa	σ_v = 800 kPa	σ_v = 1200 kPa	σ_v = 1600 kPa
1	0	0	1.5	15	1.567	1.582	1.496	1.368	1.284	1.218	1.136	1.079	1.061	0.689
2	0	0.1	1.5	15	1.497	1.474	1.393	1.269	1.192	1.132	1.055	1.002	0.932	0.886
3	0	0.5	1.5	15	1.385	1.371	1.318	1.216	1.151	1.107	1.036	0.989	0.929	0.878
4	0	1	1.5	15	1.337	1.325	1.282	1.192	1.133	1.092	1.022	0.979	0.916	0.87
5	30	0	1.5	15	1.204	1.179	1.112	1.007	0.946	0.903	0.831	0.784	0.714	0.67
6	30	0.1	1.5	15	1.152	1.140	1.071	0.968	0.91	0.868	0.798	0.754	0.688	0.649
7	30	0.5	1.5	15	1.148	1.131	1.066	0.972	0.917	0.877	0.809	0.768	0.705	0.665
8	30	1	1.5	15	1.091	1.075	1.012	0.921	0.867	0.829	0.758	0.715	0.649	0.608
9	70	0	1.5	15	0.714	0.704	0.682	0.647	0.623	0.599	0.549	0.521	0.476	0.446
10	70	0.1	1.5	15	0.779	0.767	0.746	0.708	0.678	0.651	0.601	0.573	0.528	0.5
11	70	0.5	1.5	15	0.788	0.777	0.758	0.72	0.672	0.64	0.592	0.562	0.519	0.491
12	70	1	1.5	15	0.771	0.765	0.751	0.727	0.694	0.662	0.611	0.581	0.539	0.509
13	90	0	1.5	15	0.748	0.744	0.734	0.723	0.717	0.711	0.702	0.697	0.687	0.677
14	90	0.1	1.5	15	0.696	0.689	0.677	0.664	0.657	0.65	0.641	0.633	0.619	0.609
15	90	0.5	1.5	15	0.743	0.739	0.728	0.718	0.711	0.707	0.699	0.692	0.683	0.674
16	90	1	1.5	15	0.74	0.732	0.72	0.709	0.703	0.697	0.69	0.685	0.676	0.668

infiltrated by salt solution with different concentrations under constant stress of 25 kPa, and the compression curve (e-$\log_{10}\sigma_v$) of the samples after fully saturated. It can be seen that the swelling of bentonite-sand mixtures decreases with the increase of sand content and with the increase of salt solution concentration: the void ratio of pure bentonite and bentonite-sand mixture with 30% sand content increases after fully saturated by salt solution, and the increase of void ratio decreases gradually with the increase of solution concentration; when the sand content is 70% and 90%, the swelling of mixture does not even occur due to wetting under vertical stress of 25 kPa, and the e-$\log_{10}\sigma_v$ curves of the mixture infiltrated by salt solution with different concentrations basically coincide, indicating that when the sand content is large, the solution concentration has no obvious effect on the deformation of bentonite-sand mixtures. The compression data of bentonite-sand mixtures after full swelling are shown in Table 4.

Sun et al. (2009) observed that the $\log_{10}e_m$-$\log_{10}\sigma_v$ relationship of bentonite-sand mixtures saturated by distilled water presented a unique linear relationship when the sand content is less than the critical sand content. The montmorillonite void ratio e_m is the ratio of the liquid volume V_w at full saturation to montmorillonite volume V_m, which characterizes the liquid mass absorbed by montmorillonite per unit volume after fully saturated. The critical sand content α_s is defined as the sand content that a sand skeleton will not be formed in the bentonite-sand mixture under any external stress. The montmorillonite void ratio e_m and critical sand content α_s are expressed as follows (Sun et al., 2017):

$$e_m = \frac{V_w}{V_m} = \frac{e\rho_m}{\rho(1-\alpha)\beta} \tag{1}$$

$$\alpha_s = \frac{\beta\rho_s + \frac{(1-\beta)\rho_m\rho_s}{\rho_{nm}}}{e_{smax}\rho_m + \beta\rho_s + \frac{(1-\beta)\rho_m\rho_s}{\rho_{nm}}} \tag{2}$$

where e is the void ratio at full saturation; β is the montmorillonite content in bentonite; ρ, ρ_m, ρ_{nm} and ρ_s are the densities of mixtures, montmorillonite, non-montmorillonite and sand, respectively; and e_{smax} is the maximum sand void ratio, and can be obtained through the maximum void ratio test.

When considering the effect of salt solution on HM behaviour of bentonite, the concept of true effective stress in Rao et al. (2017) is adopted. The stress on bentonite under salt solution infiltration is called the true effective stress p_e, and can be expressed as

$$p_e = (\sigma_v - u_w) + (1-\alpha)p_\pi \tag{3}$$

where u_w is the pore water pressure, and it equals 0 for the saturated sample in the steady state; p_π is the osmotic stress, which is significantly dependent on the equilibrium solution's concentration and the surface fixed charge density (Wei, 2014; Xu et al., 2014).

Fig. 3 shows the $\log_{10}e_m$-$\log_{10}p_e$ relationship of bentonite-sand mixtures with different sand contents saturated by salt solutions with different concentrations. It can be seen from Fig. 3 that the deformation data of pure bentonite and the mixtures with 30% sand content are normalized with respect to sand content and salt solution concentration using $\log_{10}e_m$-$\log_{10}p_e$ plot, and presents a linear relationship. The deformation data of the bentonite-sand mixture with 70% or 90% sand content can also be normalized with respect to salt solution concentration. In addition, for the bentonite-sand mixture with 70% or 90% sand content, when the true effective stress is greater than a certain value, the relationship

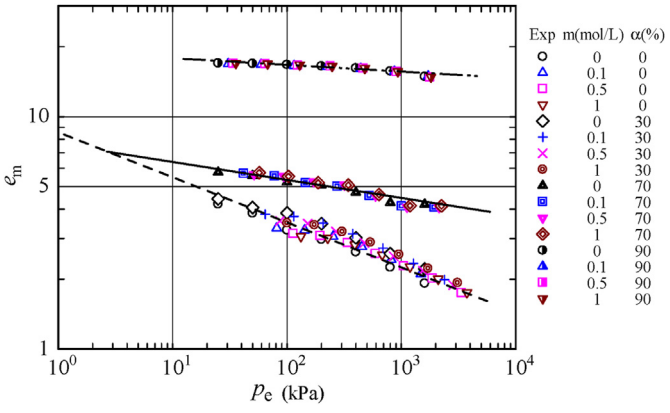

Fig. 3. $\log_{10}e_m$-$\log_{10}p_e$ relationship of bentonite-sand mixtures with different sand contents saturated by salt solution with different concentrations.

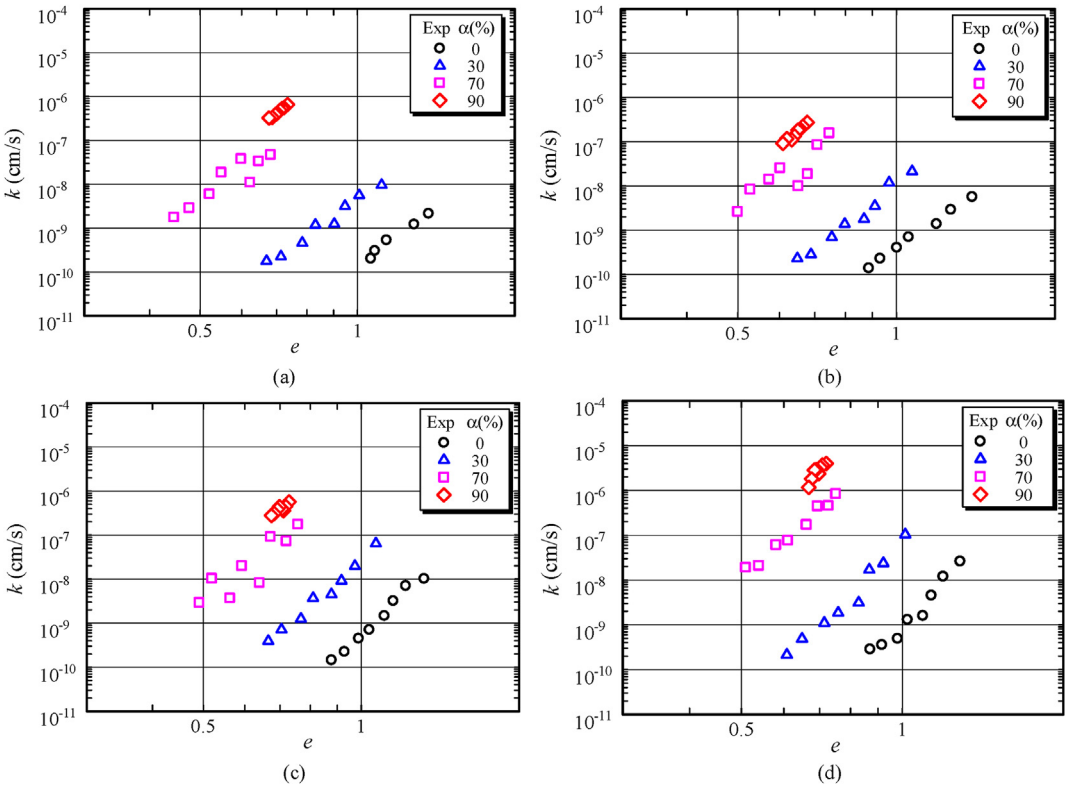

Fig. 4. $\log_{10}k$-$\log_{10}e$ relationship of bentonite-sand mixtures: (a) $m = 0$ mol/L, (b) $m = 0.1$ mol/L, (c) $m = 0.5$ mol/L, and (d) $m = 1$ mol/L.

between the montmorillonite void ratio and true effective stress deviates from the above-mentioned $\log_{10}e_m$-$\log_{10}p_e$ linear relationship. The deviation is mainly due to the formation of sand skeleton. The critical content α_s is used to judge when the sand skeleton is formed (Sun et al., 2009). The above conclusions are similar to those obtained by Sun et al. (2015b, 2017). The crucial distinction is that the *x*-coordinate is the true effective stress instead of the effective stress.

2.2.2. Permeability of bentonite-sand mixtures saturated by salt solution

Fig. 4 shows the $\log_{10}k$-$\log_{10}e$ relationship of bentonite-sand mixtures with different sand contents after saturated by deionized water or salt solution with different concentrations (m = 0 mol/L, 0.1 mol/L, 0.5 mol/L and 1 mol/L). The data of permeability coefficient of the mixture calculated by indirect method derived from consolidation theory are shown in Table 5. It can be seen that k increases approximately linearly with the increase of e for the mixture with a constant sand content; when the void ratio is the same, the higher the sand content is, the greater the permeability coefficient is. Shirazi et al. (2010) investigated the permeability coefficient using direct and indirect test methods derived from consolidation theory. Sun et al. (2014) conducted a series of compression tests on saturated bentonite prepared by deionized water, and obtained the calculated permeability coefficient. The relationship between permeability coefficient and void ratio obtained by Shirazi et al. (2010) and Sun et al. (2014) shows consistency with the $\log_{10}k$-$\log_{10}e$ relationship in Fig. 4a.

Fig. 5 presents the $\log_{10}k$-$\log_{10}e_m$ relationship of bentonite-sand mixtures. It is observed that for pure bentonite and bentonite-sand mixture with 30% sand content infiltrated by the salt solution with the same concentration, e_m is linearly correlated with k in the double logarithmic coordinates. The deviation occurs when the sand content is 70% and is more obvious at sand content of 90%.

Four groups of the $\log_{10}k$-$\log_{10}e_m$ relationship of bentonite-sand mixtures saturated by salt solutions with different concentrations are shown in Fig. 5. The $\log_{10}k$-$\log_{10}e_m$ relationship of pure bentonite and bentonite-sand mixtures with 30% sand content is linear in Fig. 5. The critical sand content for the studied bentonite-sand mixture is 46.6% according to Eq. (2). It can be observed that the $\log_{10}k$-$\log_{10}e_m$ data of mixtures with $\alpha > \alpha_s$, such as 70% and 90%, deviated from the linear relationship of pure bentonite and 30% sand content, and for this kind of bentonite with the montmorillonite content of 45.8%, the k-e_m relationship of mixtures with 70% or 90% sand content ($\alpha > \alpha_s$) is not closely tied with the salt solution concentration.

Four groups in Fig. 5 are organized in one $\log_{10}k$-$\log_{10}e_m$ diagram, as shown in Fig. 6. It can be observed that the k-e_m relationship of mixtures with 70% or 90% sand content ($\alpha > \alpha_s$) is not closely tied with the salt solution concentration.

For pure bentonite and bentonite-sand mixture with 30% sand content, due to the sand content is less than α_s, the e_m-k relationship is obviously affected by the salt solution concentration, as shown in Fig. 7. It can be observed that in the double logarithmic coordinates, the k-e_m relationship for bentonite-sand mixtures saturated with sand content less than α_s by salt solutions of same concentrations is linear, and with increase in the salt solution concentration, the slope of e_m-k linear relationship of saturated samples with sand content less than α_s increases gradually, and the permeability coefficient of bentonite-sand mixture also increases. The reason for this phenomenon is that under the action of salt solution, the thickness of double-electric layer of bentonite decreases (Rao and Mathew, 1995), and the double-electric layer thickness decreases with the increase of salt solution

Table 5
Permeability coefficient calculated by indirect method derived from consolidation theory.

No.	α (%)	m (mol/L)	ρ_{d0} (g/cm^3)	w_0 (%)	k (cm/s)							
					$\sigma_v = 100$ kPa	$\sigma_v = 200$ kPa	$\sigma_v = 300$ kPa	$\sigma_v = 400$ kPa	$\sigma_v = 600$ kPa	$\sigma_v = 800$ kPa	$\sigma_v = 1200$ kPa	$\sigma_v = 1600$ kPa
1	0	0	1.5	15		2.16×10^{-9}	1.23×10^{-9}		5.37×10^{-10}	3.07×10^{-10}	2.04×10^{-10}	
2	0	0.1	1.5	15	5.64×10^{-9}	2.91×10^{-9}	1.38×10^{-9}		7.00×10^{-10}	4.04×10^{-10}	2.29×10^{-10}	1.38×10^{-10}
3	0	0.5	1.5	15	1.03×10^{-8}	7.10×10^{-9}	3.22×10^{-9}	1.48×10^{-9}	7.10×10^{-10}	4.52×10^{-10}	2.26×10^{-10}	1.46×10^{-10}
4	0	1	1.5	15	2.62×10^{-8}	1.20×10^{-8}	4.56×10^{-9}	1.60×10^{-9}	1.30×10^{-9}	4.93×10^{-10}	3.58×10^{-10}	2.87×10^{-10}
5	30	0	1.5	15	9.64×10^{-9}	5.64×10^{-8}	3.19×10^{-9}	1.25×10^{-9}	1.19×10^{-9}	4.63×10^{-10}	2.26×10^{-10}	1.78×10^{-10}
6	30	0.1	1.5	15	2.13×10^{-8}	1.19×10^{-8}	3.51×10^{-9}	1.79×10^{-9}	1.37×10^{-9}	6.93×10^{-10}	2.82×10^{-10}	2.28×10^{-10}
7	30	0.5	1.5	15	6.48×10^{-8}	1.99×10^{-8}	9.21×10^{-9}	4.51×10^{-9}	3.72×10^{-9}	1.26×10^{-9}	7.17×10^{-10}	3.92×10^{-10}
8	30	1	1.5	15	1.04×10^{-7}	2.37×10^{-8}	1.70×10^{-8}	3.12×10^{-9}	1.86×10^{-9}	1.10×10^{-9}	4.86×10^{-10}	2.14×10^{-10}
9	70	0	1.5	15	4.70×10^{-8}	3.35×10^{-8}	1.11×10^{-8}	3.82×10^{-8}	1.86×10^{-8}	6.01×10^{-9}	2.88×10^{-9}	1.77×10^{-9}
10	70	0.1	1.5	15	1.56×10^{-7}	8.44×10^{-8}	1.86×10^{-8}	9.97×10^{-9}	2.53×10^{-8}	1.40×10^{-8}	8.33×10^{-9}	2.61×10^{-9}
11	70	0.5	1.5	15	1.76×10^{-7}	7.27×10^{-8}	9.19×10^{-8}	8.28×10^{-9}	2.00×10^{-8}	3.71×10^{-9}	1.04×10^{-8}	2.94×10^{-9}
12	70	1	1.5	15	4.90×10^{-8}	3.66×10^{-8}	3.25×10^{-8}	1.24×10^{-8}	3.23×10^{-8}	6.72×10^{-9}	9.27×10^{-9}	3.86×10^{-9}
13	90	0	1.5	15	6.55×10^{-7}	5.60×10^{-7}	5.30×10^{-7}	4.88×10^{-7}	4.16×10^{-7}	3.91×10^{-7}	3.34×10^{-7}	3.24×10^{-7}
14	90	0.1	1.5	15	2.72×10^{-7}	2.22×10^{-7}	1.91×10^{-7}	1.81×10^{-7}	1.35×10^{-7}	1.10×10^{-7}	1.17×10^{-7}	9.13×10^{-8}
15	90	0.5	1.5	15	5.68×10^{-7}	4.51×10^{-7}	3.58×10^{-7}	3.95×10^{-7}	4.44×10^{-7}	3.85×10^{-7}	3.10×10^{-7}	2.78×10^{-7}
16	90	1	1.5	15	4.11×10^{-7}	2.21×10^{-7}	2.82×10^{-7}	3.75×10^{-7}	2.67×10^{-7}	2.74×10^{-7}	2.46×10^{-7}	2.18×10^{-7}

concentration, the colloid structure of bentonite collapses, the flow channel among soil particles increases, and finally the permeability of bentonite-sand mixtures increases.

2.3. Test results of deformation and permeability in the literature

2.3.1. Deformation

Karnland et al. (2008) studied the swelling deformation of pure MX80 bentonite and its mixture with 30% sand content saturated by salt solution with different concentrations. The deformation data are reorganized by the montmorillonite void ratio e_m and true effective stress p_e, as shown in Fig. 8. It can be observed that the relationship between e_m and p_e of bentonite-sand mixtures with $\alpha = 0\%$ and 30%, less than $\alpha_s = 49.3\%$, is linear in the double logarithmic coordinates.

Mollins et al. (1996) and Studds et al. (1998) carried out the swelling deformation tests on Wyoming bentonite-sand mixtures with different sand contents infiltrated by distilled water and salt solutions with different concentrations, respectively. The deformation data of Mollins et al. (1996) and Studds et al. (1998) are reorganized by e_m and p_e relationship, as shown in Fig. 9. The e_m-p_e relationship of pure Wyoming bentonite shows the linear

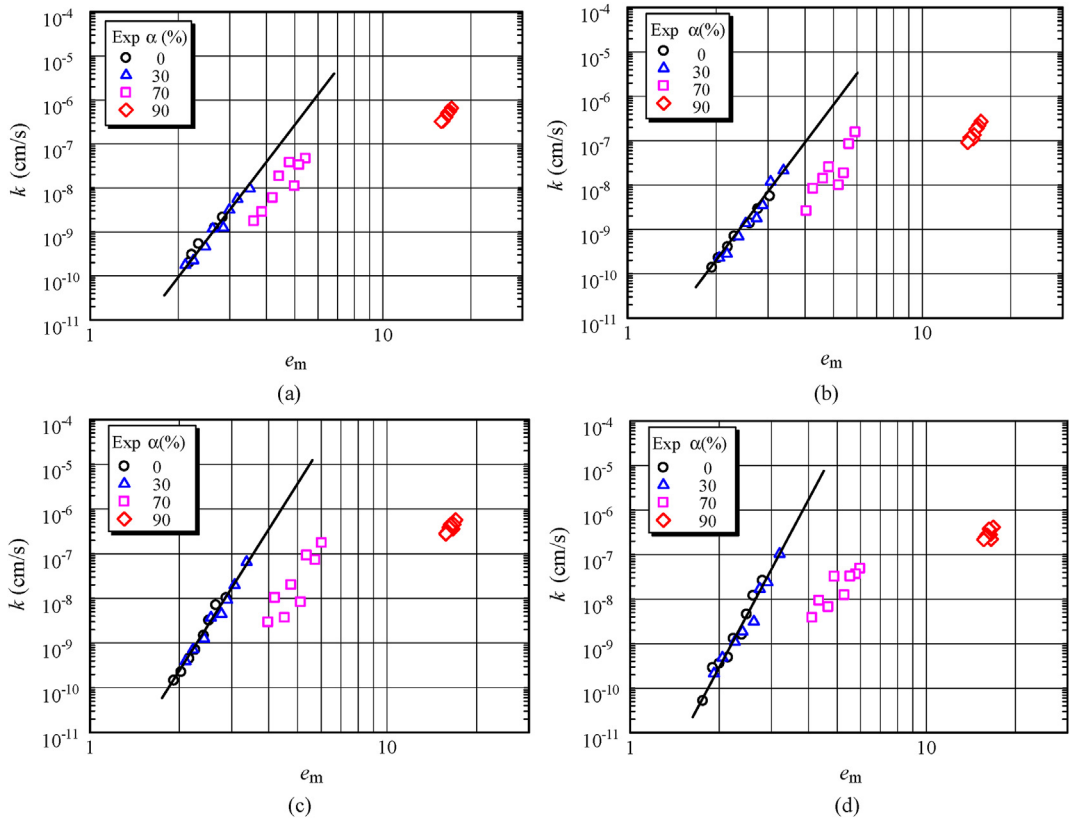

Fig. 5. $\log_{10}k$-$\log_{10}e_m$ relationship of bentonite-sand mixtures saturated by salt solutions with different concentrations: (a) $m = 0$ mol/L, (b) $m = 0.1$ mol/L, (c) $m = 0.5$ mol/L, and (d) $m = 1$ mol/L.

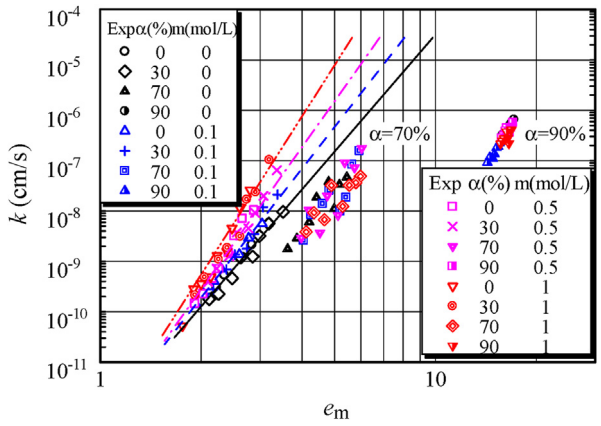

Fig. 6. $\log_{10}k$-$\log_{10}e_m$ relationship of bentonite-sand mixtures.

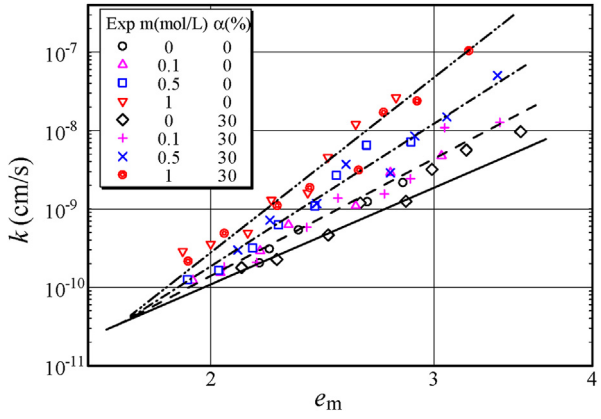

Fig. 7. $\log_{10}k$-$\log_{10}e_m$ relationship of bentonite-sand mixtures ($\alpha \le \alpha_s$) saturated by salt solution with different concentrations.

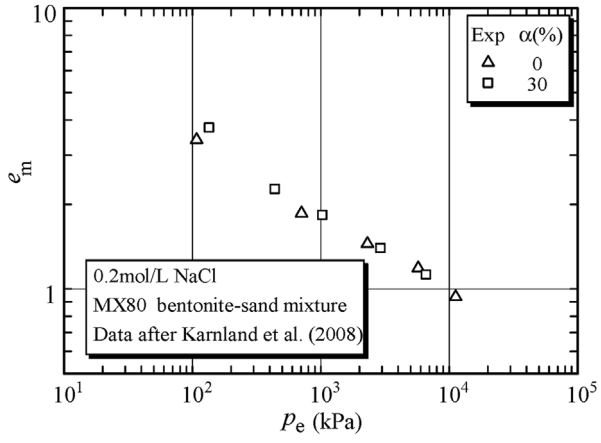

Fig. 8. $\log_{10}e_m$-$\log_{10}p_e$ relationship of MX80 bentonite-sand mixtures with $\alpha \le \alpha_s$ infiltrated by salt solution.

correlation, and the deviation occurs when the sand contents are 80%, 90% and 95%. From Fig. 9b, it can also be found that the effect of salt solution concentration on the swelling deformation of the mixtures with different sand contents can be negligible.

2.3.2. Permeability

Ye et al. (2014) measured the saturated permeability coefficient of pure GMZ01 bentonite infiltrated by salt solution with different concentrations. Fig. 10 shows the $\log_{10}k$-$\log_{10}e_m$ relationship. It can be seen that the $\log_{10}k$-$\log_{10}e_m$ relationship of GMZ01 bentonite infiltrated by salt solution with different concentrations is linear, and the slope of the $\log_{10}k$-$\log_{10}e_m$ relation line increases with increasing salt solution concentration. Moreover, the $\log_{10}k$-$\log_{10}e_m$ relation lines of GMZ01 bentonite infiltrated by salt solution with different concentrations intersect at the same point.

Studds et al. (1998) conducted the permeability tests for pure Wyoming bentonite and its mixture with the sand contents of 80% and 90% infiltrated by distilled water and 0.1 mol/L salt solution. Fig. 11 shows the $\log_{10}k$-$\log_{10}e_m$ relationship. It can be observed that the $\log_{10}k$-$\log_{10}e_m$ relationship of pure bentonite infiltrated by distilled water or 0.1 mol/L salt solution is linear. The latter has a higher slope than the former, and the two lines intersect at one point, which is consistent with the rules shown in Fig. 10. When the sand content is 80% or 90%, the $\log_{10}k$-$\log_{10}e_m$ relationship deviates from the $\log_{10}k$-$\log_{10}e_m$ line of pure bentonite, and the greater the sand content is, the more obvious the deviation is. Moreover, the $\log_{10}k$-$\log_{10}e_m$ relationship after the deviation presents the roughly bi-linear relation. At the first stage, the slope of $\log_{10}k$-$\log_{10}e_m$

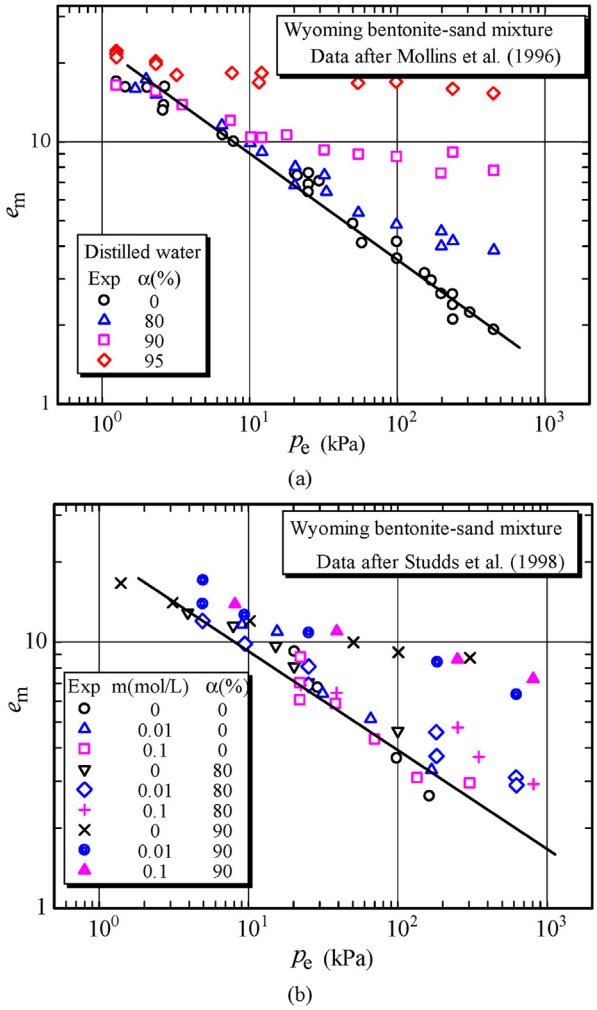

Fig. 9. $\log_{10}e_m$-$\log_{10}p_e$ relationship of Wyoming bentonite-sand mixtures infiltrated by distilled water or salt solution: (a) Data from Mollins et al. (1996), and (b) Data from Studds et al. (1998).

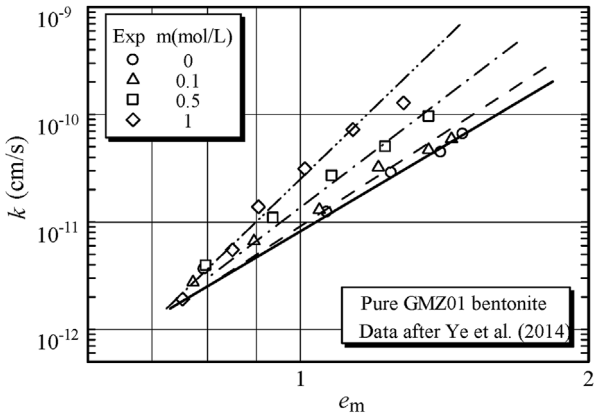

Fig. 10. $\log_{10}k$-$\log_{10}e_m$ relationship of GMZ01 bentonite saturated by salt solution with different concentrations.

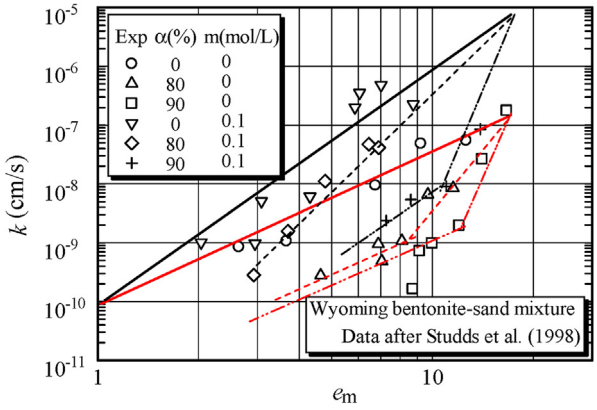

Fig. 11. $\log_{10}k$-$\log_{10}e_m$ relationship of Wyoming bentonite and its sand mixture ($\alpha > \alpha_s$).

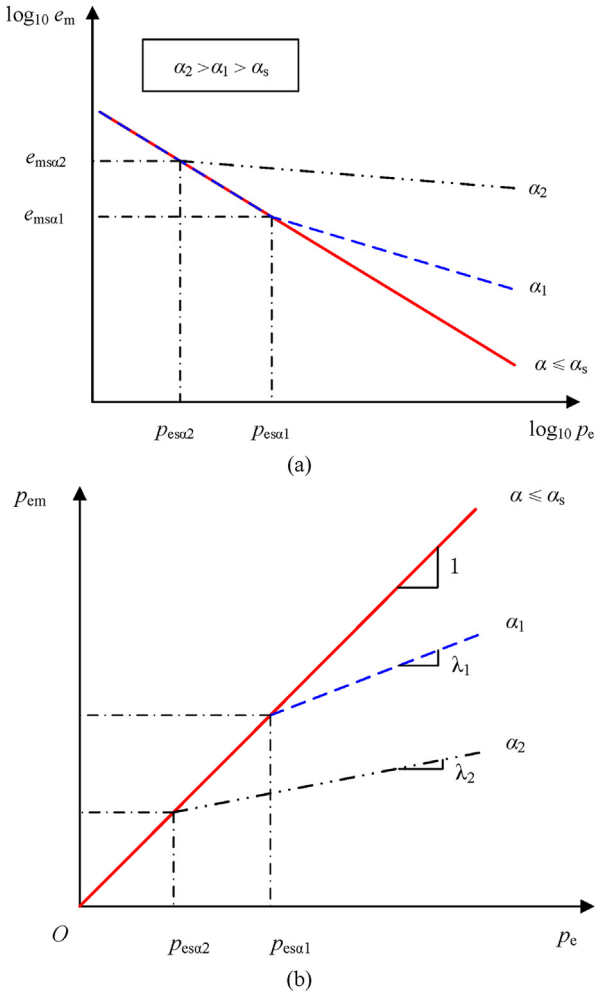

Fig. 12. Deformation prediction model of bentonite-sand mixtures under salt solution infiltration ($\alpha_2 > \alpha_1 > \alpha_s$): (a) $\log_{10}e_m$-$\log_{10}p_e$, and (b) p_{em}-p_e.

relation line increases with increasing sand content. At the second stage, the slope of $\log_{10}k$-$\log_{10}e_m$ relation line is almost the same as that of pure bentonite infiltrated by the salt solution with the same concentration. The $\log_{10}k$-$\log_{10}e_m$ relation lines of the mixtures with 80% or 90% sand content infiltrated by salt solution with different concentrations do not coincide with each other, which is different with the $\log_{10}k$-$\log_{10}e_m$ relationship of the mixtures with $\alpha > \alpha_s$, as shown in Fig. 6. The reason may be related to the higher montmorillonite content of Wyoming bentonite of about 80%.

To sum up, the $\log_{10}e_m$-$\log_{10}p_e$ and $\log_{10}k$-$\log_{10}e_m$ relationships can reflect the deformation and permeability respectively of different types of bentonite and its sand mixture infiltrated by the salt solution with different concentrations. Therefore, according to above experimental rules, the model for predicting the HM behaviour of bentonite-sand mixtures under coupled MC effect can be established.

3. HM behaviour prediction model of bentonite-sand mixture under salt solution infiltration

3.1. Swelling prediction model

Based on the above swelling characteristics analysis, it is known that the e_m-p_e relationship of bentonite-sand mixtures saturated by salt solution can be normalized with respect to salt solution concentration. Therefore, the swelling prediction model of bentonite-sand mixture in a full range of sand content under the salt solution infiltration is shown in Fig. 12, in which p_{em} is defined as the true effective stress borne by montmorillonite alone.

It displays similar to the swelling prediction model of bentonite-sand mixture infiltrated by distilled water (Sun et al., 2015b, 2017), with the main difference of abscissa of the true effective stress instead of the effective stress, considering the effect of salt solution concentration. Specifically, in the swelling prediction model of bentonite-sand mixture infiltrated by salt solution, when the sand content α is less than or equal to the critical sand content α_s, the sand skeleton will not be formed, and the unique linear relationship of e_m-p_e with the slope of b_0 in a double logarithmic e_m-p_e coordinates will be consistently satisfied, which can be expressed as follows:

$$\log_{10}e_m = a_0 - b_0\log_{10}p_e \tag{4}$$

where a_0 and b_0 are the material parameters varying with types of bentonite, and can be determined by the two swelling tests on pure bentonite samples under any vertical stress.

Moreover, a sand skeleton will not form at this time, and therefore the true effective vertical stress is borne by montmorillonite alone, i.e. $p_{em} = p_e$, and the stress distribution ratio $\lambda = 1$; when p_e is larger than the true effective deviatoric stress $p_{es\alpha}$, p_{em} is

assumed to increase linearly with p_e and the slope is λ, as shown in Fig. 12b.

When α is greater than α_s, taking the mixture with a sand content $\alpha = \alpha_1$ as an example, the e_m-p_e relation of bentonite-sand mixture deviates from the unique linear e_m-p_e relationship, and presents a bi-linear relation with $p_{es\alpha}$ as the intersection. The phenomena of deviation shown in Fig. 12a can be attributed to the formation of a sand skeleton in bentonite–sand mixtures.

According to the test results, a sand skeleton will form when the void ratio of sand in the mixture is equal to the maximum sand void ratio e_{smax} (Sun et al., 2009). Meanwhile, sand particles just make contact in mixtures when the vertical true effective stress equals $p_{es\alpha}$, and at this time the montmorillonite void ratio equals $e_{ms\alpha}$, as shown in Fig. 12a. Moreover, $e_{ms\alpha}$ and $p_{es\alpha}$ were satisfied with the linear e_m-p_e relationship, as shown in Eq. (4), and therefore, the true effective deviatoric stress $p_{es\alpha}$ can be expressed as follows:

$$\log_{10}\frac{p_{es\alpha}}{p_a} = \frac{1}{b_0}\left\{a_0 - \log_{10}\left\{\frac{\alpha\rho_m}{(1-\alpha)\beta\rho_s}e_{sm\alpha x} - \left[1+\frac{(1-\beta)\rho_m}{\beta\rho_{nm}}\right]\right\}\right\} \tag{5}$$

where p_a is the atmospheric pressure of 100 kPa.

When the true effective stress is less than or equal to the true effective deviatoric stress, i.e. $p_e \le p_{es\alpha}$, the sand skeleton is not formed, and the e_m-p_e linear relationship (i.e. Eq. (4)) is still satisfied; when $p_e > p_{es\alpha}$, the sand skeleton is formed, and the e_m-p_e relationship begins to deviate from the e_m-p_e relation line, and shows another linear relationship with the slope of b_α. Meanwhile, the point ($p_{es\alpha}$, $e_{ms\alpha}$) is the end of the deviated e_m-p_e relation line, as shown in Fig. 12. Therefore, the linear e_m-p_e relationship when $p_e > p_{es\alpha}$ can be expressed as follows:

$$\log_{10}e_m = \log_{10}e_{ms\alpha} - b_\alpha\log_{10}(p_e / p_{es\alpha}) \tag{6}$$

where $e_{ms\alpha}$ is the montmorillonite void ratio corresponding to $p_{es\alpha}$, and the point ($p_{es\alpha}$, $e_{ms\alpha}$) is the intersection where e_m-p_e relationship begins to deviate from the e_m-p_e relation line; b_α is the slope of e_m-p_e line after deviation, related to the sand content α and montmorillonite content β in bentonite.

The deformation data of bentonite-sand mixtures are normalized with respect to salt solution, consequently the e_m-p_e relation after the deviation can be obtained by the method in Sun et al. (2017), i.e. after determining the stress distribution ratio λ between bentonite and sand skeleton, the true effective stress borne by bentonite can be determined. Afterwards, according to the rule for the montmorillonite void ratio and the true effective stress borne by montmorillonite is satisfied with the unique linear relationship, the montmorillonite void ratio corresponding to true effective stress can be obtained.

Once the e_m-p_e relationship is determined, the relationship between the final void ratio and the vertical stress (e_f-p_e) after full wetting for mixtures with a specified sand content can be obtained. According to the e_f-p_e relationship, the deformation after full wetting (swelling or collapse) under any true effective vertical stress can be judged for mixtures at any initial state. In practical engineering, bentonite-sand mixture is also in a constant volume state, i.e. the void ratio keeps almost unchanged as the initial void ratio e_0 (Sun and Sun, 2016). From the e_f-p_e relationship, the swelling pressure p_s of mixture can be obtained. When the mixture undergoes a vertical stress greater than p_s, the mixture is compressed; and when the mixture undergoes a vertical stress smaller than p_s, the mixture swells. The final state will reach the e_f-σ_v relationship determined from the predicted e_m-σ_v relationship.

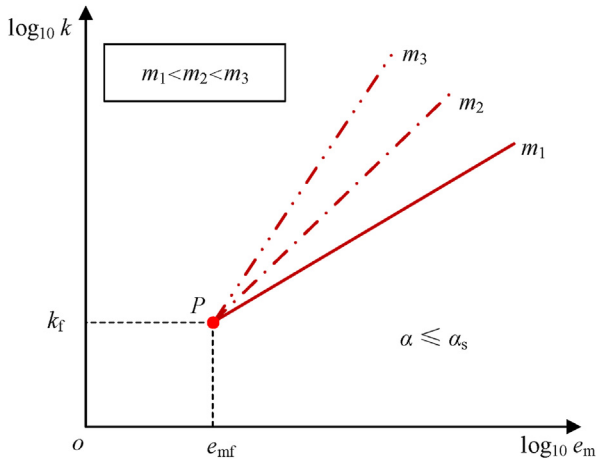

Fig. 13. Permeability prediction model due to salt solution concentration variation of bentonite-sand mixture with $\alpha \le \alpha_s$.

3.2. Permeability prediction model

Based on the permeability obtained from the k-e_m relationship, the permeability prediction model of bentonite-sand mixtures with different sand contents under infiltration of salt solution with different concentrations is established. The relationship between montmorillonite void ratio and saturated permeability coefficient of bentonite-sand mixtures can be divided into two parts.

3.2.1. Permeability prediction model due to salt solution variation of bentonite-sand mixtures with $\alpha \le \alpha_s$

Fig. 13 shows the sketch of permeability prediction model due to salt solution concentration variation of bentonite-sand mixtures with $\alpha \le \alpha_s$. Tripathi (2013) studied the permeability of bentonite under infiltration of salt solution with different concentrations and showed that the permeability coefficient of pure bentonite reached a minimum in a dense condition. The k-e_m relationship of bentonite-sand mixtures with $\alpha \le \alpha_s$ obtained in this study, as shown in Fig. 7, also indicates that the k-e_m relation lines of bentonite-sand mixtures with $\alpha \le \alpha_s$ intersect to a point. The same trend of k-e_m relationship can also be observed for pure GMZ01 bentonite in Ye et al. (2014), as shown in Fig. 10. All of the above can prove that there is a critical point P (e_{mf}, k_f) in the $\log_{10}k$-$\log_{10}e_m$ diagram, as shown in Fig. 13, where e_{mf} and k_f are the montmorillonite void ratio and saturated permeability coefficient at critical point P, respectively. The values of e_{mf} and k_f of different types of bentonite and its sand mixture are related to the montmorillonite content in bentonite, and can be obtained through the permeability tests on two groups of sand-bentonite mixtures with different void ratios. When e_m is greater than e_{mf}, the slope of the k-e_m relation line increases with increasing salt solution concentration. Therefore, the relationship between e_m and k of bentonite-sand mixtures with $\alpha \le \alpha_s$ is expressed as follows:

$$\log_{10}(k / k_f) = \eta_m\log_{10}(e_m / e_{mf}) \tag{7}$$

where η_m is the slope of the k-e_m relation line of saturated bentonite-sand mixture with $\alpha \le \alpha_s$ saturated by salt solutions with different concentrations. When the salt solution concentration is 0, we have $\eta_m = \eta_0$. The slope η_m is related to the montmorillonite content β and salt solution concentration m, and can be expressed as Eq. (8) through summarizing the permeability test data of

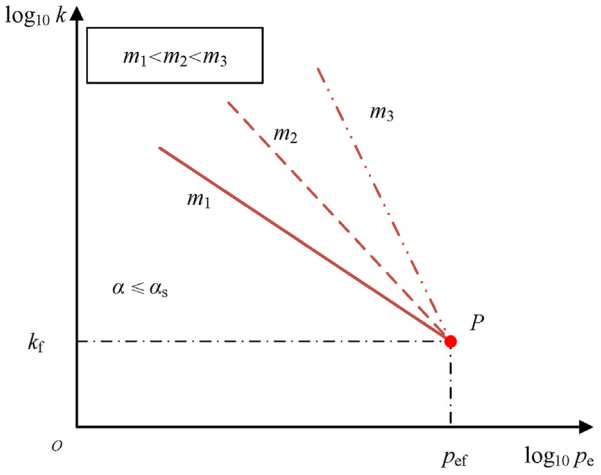

Fig. 14. $\log_{10}k$-$\log_{10}p_e$ relationship for bentonite-sand mixtures with $\alpha \le \alpha_s$ saturated by salt solution.

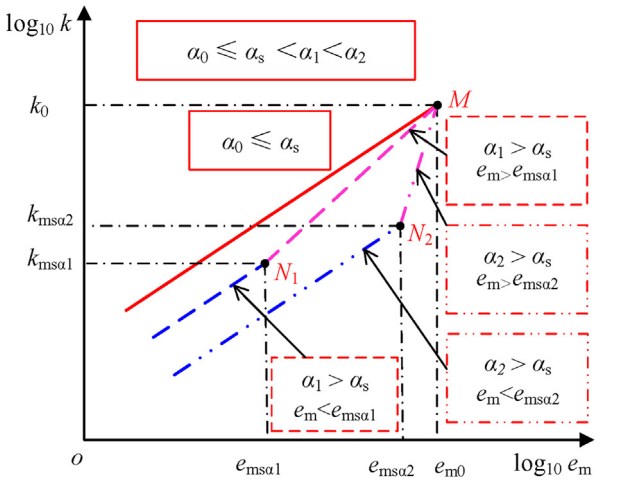

Fig. 15. Permeability prediction model of bentonite-sand mixtures saturated by salt solution (m is kept constant and α changes).

different types of bentonite and its sand mixture infiltrated by salt solution with different concentrations (Mollins et al., 1996; Studds et al., 1998; Karnland et al., 2008; Ye et al., 2014).

$$\eta_m = \frac{0.63 - 0.68\beta}{\beta^2(1-\beta)^2}m + \frac{1 - 1.1\beta}{\beta^2(1-\beta)^2} \tag{8}$$

When $\alpha \le \alpha_s$, the sand skeleton will not be formed, and unique e_m-p_e relation line expressed in Eq. (4) keeps satisfied. Combined with Eq. (7), the relationship between saturation permeability coefficient and true effective stress (k-p_e) of bentonite-sand mixtures with $\alpha \le \alpha_s$ can be established, as shown in Fig. 14, and the relationship between k and p_e is expressed as follows:

$$\log_{10}\frac{k}{k_f} = \frac{\eta_m}{b_0}\left(\log_{10}p_{ef} - b_0{}^2\log_{10}p_e\right) \tag{9}$$

where p_{ef} is the true effective stress corresponding to the critical point P. Through Eq. (9), the saturated permeability coefficient of bentonite-sand mixture with $\alpha \le \alpha_s$ under different true effective stresses and salt solution concentrations can be calculated once given the salt solution concentration, sand content, montmorillonite content, and values of a_0 and b_0.

3.2.2. Permeability prediction model due to sand content variation of bentonite-sand mixtures saturated by salt solution with constant concentration

Fig. 15 shows the sketch of permeability prediction model due to sand content variation of bentonite-sand mixtures saturated by salt solution with constant concentration.

When $\alpha \le \alpha_s$, the e_m-k relation keeps satisfying the linear relationship, with the slope of constant η_m, and obeys the expression of Eq. (7).

When $\alpha > \alpha_s$, the k-e_m relation deviates from the linear relationship, and the starting deviation point is M (e_{m0}, k_0), where e_{m0} is the montmorillonite void ratio when the true effective stress p_e is 1 kPa in deformation model, and k_0 is the permeability coefficient when $p_e = 1$ kPa in the k-p_e relationship of bentonite-sand mixtures with $\alpha \le \alpha_s$ saturated by salt solution.

When $\alpha > \alpha_s$, the k-e_m relation is approximately bi-linear. For example, the dash lines for mixture with sand content of α_1 intersect at Point N_1 and the dot dash lines for mixture with sand content of α_2 intersect at Point N_2, as shown in Fig. 15, where the abscissa values of Points N_1 and N_2 represents the montmorillonite void ratio $e_{msα}$ of the deviation point in the deformation prediction model where the e_m-p_e relationship begins to deviate from the e_m-p_e relation line, as shown in Fig. 12. It can be seen from Eqs. (4) and (5) that $e_{msα}$ is related to the montmorillonite content and sand content but is uncorrelated to the salt solution concentration. Moreover, the higher the sand content, the greater the $e_{msα}$.

At the right side of the intersection point N_1 or N_2, i.e. $e_m > e_{msα}$, the slope of the k-e_m relation line is $\eta_{mα}$, which is related to the sand content, the montmorillonite content of bentonite, and the salt solution concentration. At this part, the void ratio of the mixture is relatively large, and the pores are not filled with saturated bentonite. Therefore, the permeability of the mixtures is closely related to the sand content. The slope $\eta_{mα}$ increases with increasing sand content. For example, due to $\alpha_1 < \alpha_2$, the former slope is less than the latter. In addition, the salt solution concentration also has an impact on the saturated permeability of bentonite-sand mixtures. The swelling potential of bentonite decreases with increasing salt solution concentration (Ma et al., 2016), causing the increase of permeability coefficient of bentonite-sand mixtures. Therefore, for mixture with the same sand content, the higher the salt solution concentration, the greater the slope $\eta_{mα}$.

At the left side of the intersection N_1 or N_2, i.e. $e_m < e_{msα}$, the slope of the e_m-k relation line is supposed to equal the slope η_m of the e_m-k relation line of the mixture with $\alpha \le \alpha_s$, because in this part, the mixture is in the relatively dense state and the saturated bentonite can be completely filled with sand pores (Sun et al., 2017). Therefore, the variation of permeability of mixture with $\alpha > \alpha_s$ in this part is almost the same as that of the mixture with $\alpha \le \alpha_s$.

Therefore, the k-e_m relationship of mixture with $\alpha > \alpha_s$ can be expressed as follows:

$$\log_{10}k = \log_{10}k_0 + \eta_{mα}\log_{10}\frac{e_m}{e_{m0}} \quad (e_m \ge e_{msα}) \tag{10}$$

$$\log_{10}k = \log_{10}k_{msα} + \eta_m\log_{10}\frac{e_m}{e_{msα}} \quad (e_m < e_{msα}) \tag{11}$$

In Eq. (10), $\eta_{mα}$ is the slope of k-e_m relation line in the range of $\alpha > \alpha_s$ and $e_m \ge e_{msα}$. Fig. 16 shows the sketch of $\eta_{mα}$-α relationship. When $\alpha \le \alpha_s$, sand skeleton is not formed, and the slope of k-e_m relation line of mixture is constant, i.e. η_m. When α is close to 100%, k equals the permeability coefficient of sand, and $\eta_{mα}$ is supposed to

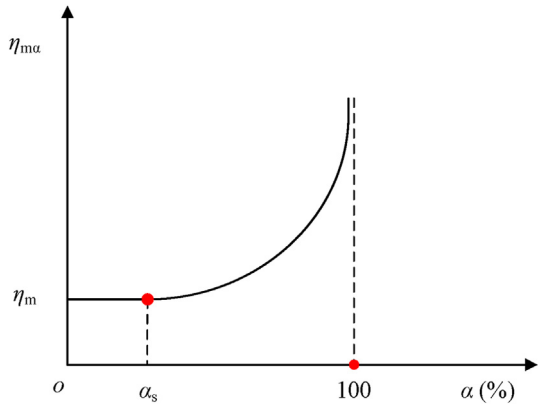

Fig. 16. Sketch of $\eta_{m\alpha}$-α relationship.

be close to infinity. When $\alpha_s \le \alpha < 100\%$, the relationship between $\eta_{m\alpha}$ and α is assumed as the downward convex parabolic relation. The reason for this assumption is that when the sand content increases gradually, the impact of bentonite on permeability of mixture decreases, while the sand does the opposite. Therefore, the slope $\eta_{m\alpha}$ of the k-e_m relation line changes slowly with the increase of the sand content at the beginning and varies rapidly. In addition, according to the published permeability data of bentonite-sand mixture (Mollins et al., 1996; Studds et al., 1998), the relationship between $\eta_{m\alpha}$ and α of different types of bentonite and its sand mixture can be summarized as follows:

$$\eta_{m\alpha} = \frac{(1.95m+1.351)(-2.42\beta+2.102)}{100\alpha^3(1-\alpha)^4} + (2.793m+6.408)(-0.968\beta+1.441) \quad (12)$$

To sum up, the sketch of permeability prediction model for bentonite-sand mixtures due to salt solution concentration and sand content variation is shown in Fig. 17. The dash line represents the case that the bentonite-sand mixture infiltrated by the salt solution with concentration of m_i, and the solid line is the case that the salt solution concentration is m_j, which is higher than m_i. When $\alpha \le \alpha_s$, the k-e_m relation line of mixtures saturated by salt solution with different concentrations intersects at the critical point P (e_{mf}, k_f) and the slope increases with increasing salt solution concentration. When $\alpha > \alpha_s$ and the salt solution concentration is m_i, the k-e_m relationship deviates from the line at point M_i, and point N_i ($e_{ms\alpha}$, $k_{ms\alpha i}$) is the intersection point of bi-linear relationship. Similarly, for the case of m_j concentration (the solid lines), point N_j ($e_{ms\alpha}$, $k_{ms\alpha j}$) is the intersection point of bi-linear relationship.

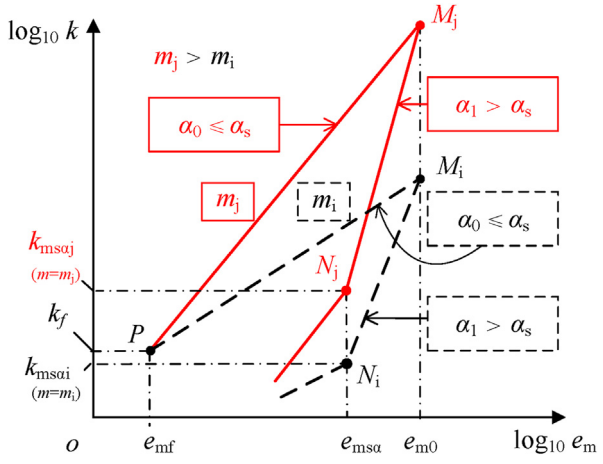

Fig. 17. Sketch of permeability prediction model for bentonite-sand mixtures due to salt solution concentration and sand content variation.

According to the permeability prediction model, the saturated permeability coefficient of bentonite-sand mixtures under external stress and saturated by the salt solution with different concentrations can be calculated, given the basic parameters of bentonite-sand mixtures, such as a_0, b_0, sand content α, montmorillonite content β, and salt solution concentration m.

4. Model verification

The prediction model is adopted to predict the deformation and saturated permeability coefficient of different types of bentonite-sand mixtures saturated by salt solution with different concentrations. The parameters required in the prediction are listed in Table 6.

4.1. Deformation prediction for bentonite-sand mixtures with different sand contents saturated by salt solution

The deformation prediction model was adopted to predict the deformation of Wyoming bentonite-sand mixture due to saturation. The predicted results are in good agreement with the deformation results of the mixtures saturated by salt solution with different concentrations in Studds et al. (1998) and by distilled water in Mollins et al. (1996), as shown in Fig. 18.

The model is also used to predict the deformation of bentonite and its sand mixture used in this study, and the predicted results are also consistent with the test results in Section 2.3 of bentonite-sand mixtures with different sand contents saturated by the salt solution with different concentrations, as shown in Fig. 19.

Table 6
Parameters of deformation and permeability prediction model for four types of bentonite and its sand mixture.

Type of mixture	ρ_m (g/cm^3)	ρ_{nm} (g/cm^3)	ρ_s (g/cm^3)	e_{smax}	a_0	b_0	β (%)	α_s (%)
Wyoming bentonite-sand mixture	2.76	2.74	2.66	0.98	1.361	0.389	85	49.3
MX80 bentonite-sand mixture	2.76	2.74	2.66	0.98	1.171	0.296	80	49.3
GMZ01-Na bentonite-sand mixture	2.79	2.78	2.66	1	0.728	0.197	75.4	49.1
GCL Bentonite-sand mixture	2.72	2.70	2.65	1	0.915	0.182	45.8	46.7

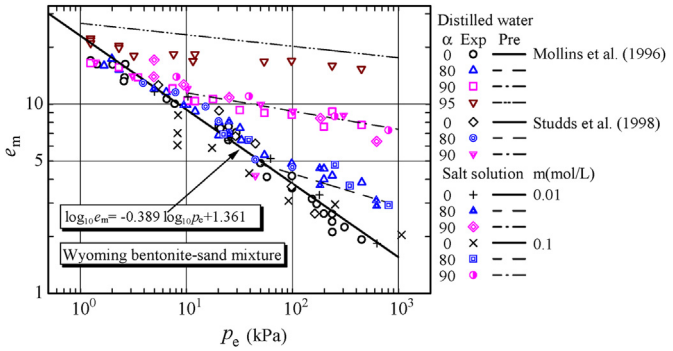

Fig. 18. Deformation prediction of Wyoming bentonite-sand mixtures.

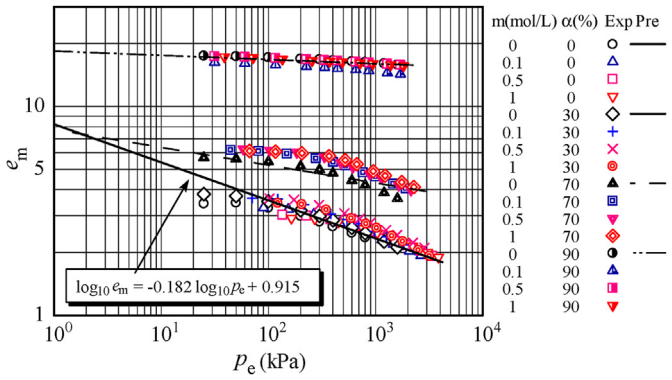

Fig. 19. Deformation prediction of GCL bentonite-sand mixtures used in the study.

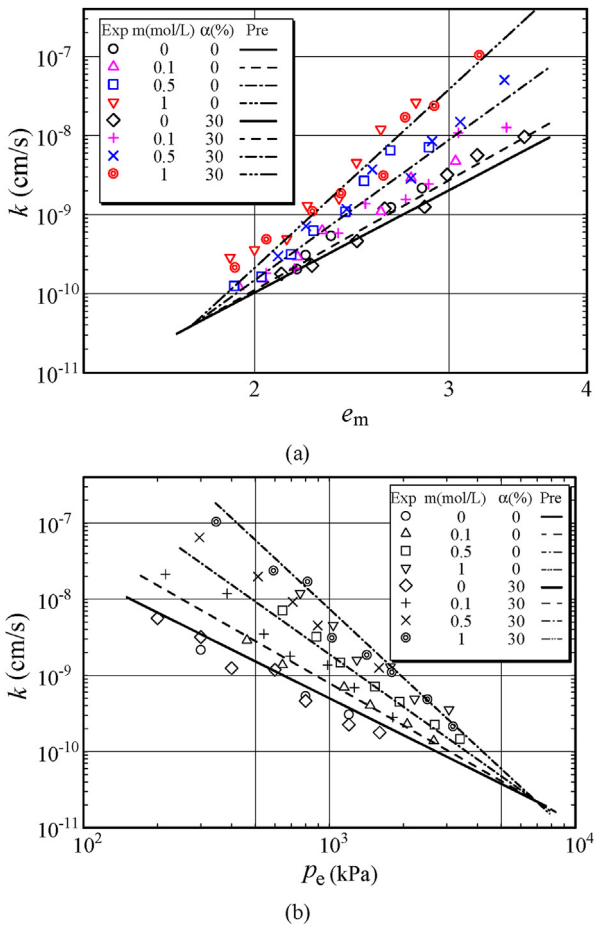

Fig. 20. Permeability prediction of GCL bentonite-sand mixtures with $\alpha \leq \alpha_s$ used in this study: (a) k-e_m, and (b) k-p_e. Pre stand for prediction.

Therefore, the deformation prediction model can be adopted to predict the deformation of different types of bentonite and its sand mixture saturated by salt solution.

4.2. Permeability prediction model of bentonite-sand mixtures

The permeability prediction model is adopted to predict the saturated permeability coefficient of bentonite-sand mixtures with $\alpha \leq \alpha_s$ saturated by salt solution with different concentrations. The predicted results are in good agreement with the measured

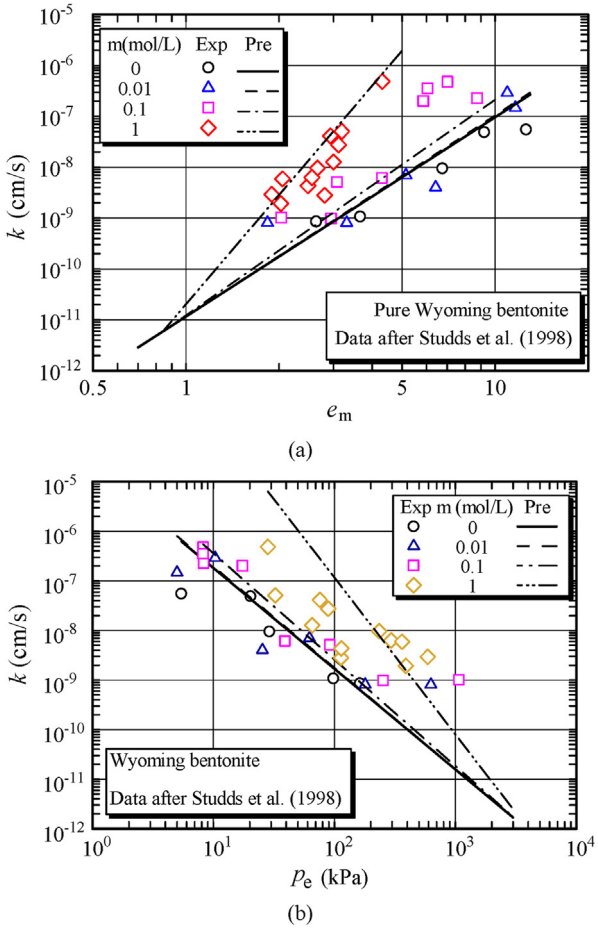

Fig. 21. Permeability prediction of Wyoming pure bentonite saturated by salt solution with different concentrations: (a) k-e_m, and (b) k-p_e.

permeability results in terms of k-e_m and k-p_e relationships of different types of bentonite and its sand mixture with $\alpha \leq \alpha_s$, such as GCL bentonite and its sand mixture in this study, as shown in Fig. 20, Wyoming bentonite (Studds et al., 1998) in Fig. 21, GMZ01 pure bentonite (Ye et al., 2014) in Fig. 22, and MX80 pure bentonite (Karnland et al., 2008) in Fig. 23.

From Figs. 20–23, it can be concluded that the permeability prediction model can be used to predict the saturated permeability coefficient of different types of bentonite and its sand mixture with $\alpha \leq \alpha_s$. Moreover, the predicted k-p_e relationship is more convenient for practical application.

The k-e_m relationship of bentonite-sand mixtures with $\alpha > \alpha_s$ saturated by the salt solution with different concentrations is predicted using the permeability prediction model, such as Wyoming bentonite and its mixture in Studds et al. (1998), as shown in Fig. 24, and GCL bentonite and its mixture used in the study, as shown in Fig. 25. It can be seen that the permeability prediction results are basically consistent with experimental results.

From Figs. 20–25, it can be concluded that the permeability prediction model can be used to predict the saturated permeability coefficient of different types of bentonite and its sand mixture at a full range of sand content saturated by salt solutions with different concentrations.

To sum up, the proposed swelling and permeability prediction model can comprehensively reflect the HMC behaviour of bentonite-sand mixtures, i.e. it can predict not only the swelling

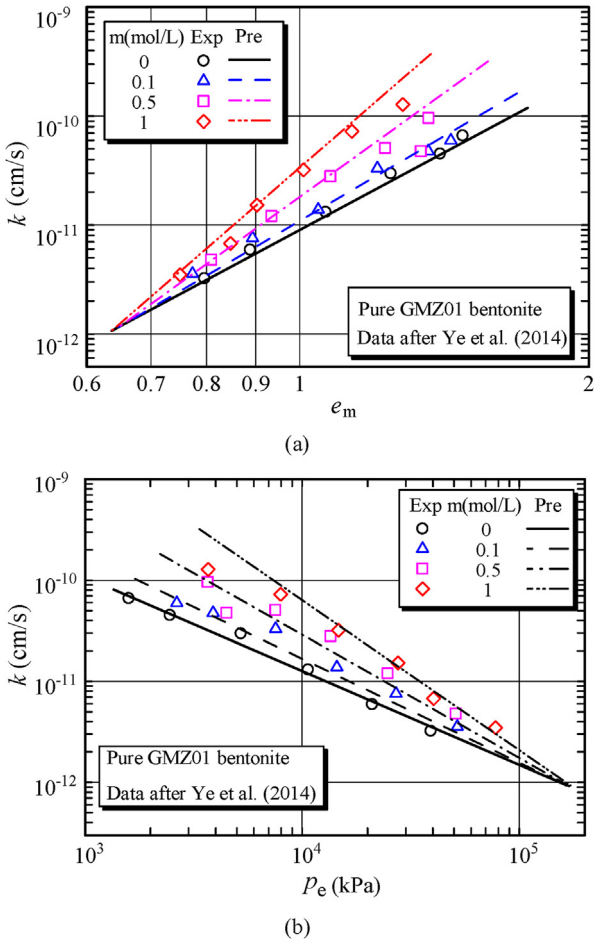

Fig. 22. Permeability prediction of pure GMZ01 bentonite saturated by salt solution with different concentrations: (a) k-e_m, and (b) k-p_e.

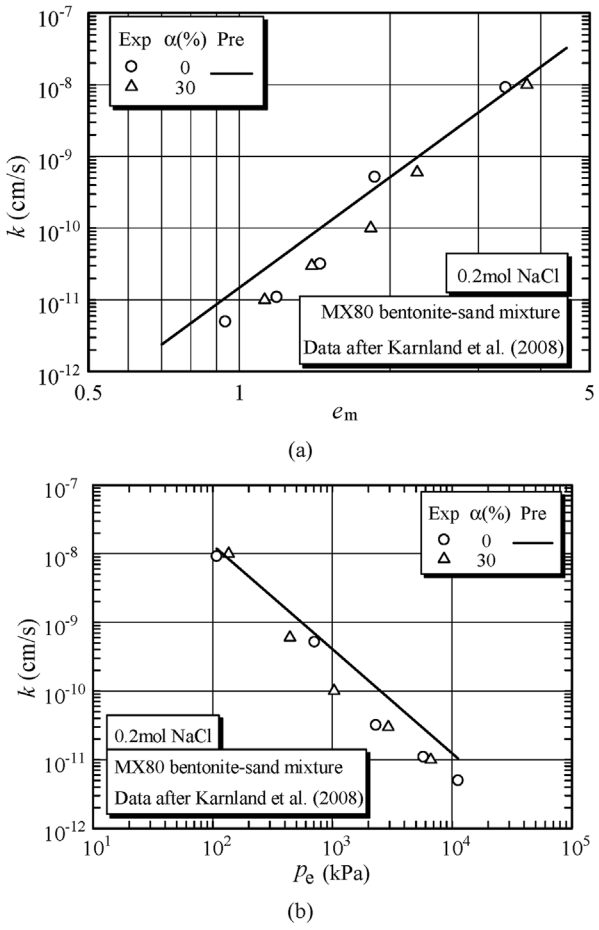

Fig. 23. Permeability prediction of pure MX80 bentonite and its mixture with 30% sand content: (a) k-e_m, and (b) k-p_e.

characteristics including swelling deformation (swelling or collapse) and swelling pressure, but also the saturated permeability of bentonite-sand mixture at a full range of sand content under the salt solution infiltration with different concentrations.

Meanwhile, the type of bentonite, the initial dry density and the optimum bentonite-sand mixing ratio can also be determined according to the proposed model once given the environmental groundwater salt concentration, the vertical pressure, the maximum allowable swelling pressure, and the anti-seepage requirements allowed by local regulations. To be specific, it is different in permeability coefficient required by the impermeable isolation layer of landfill and the buffer/backfill barrier of HLW repository. In the deep geological disposal, the allowable swelling pressure of bentonite-sand mixture ought to be confined considering the integrity of surrounding rock barrier. Moreover, the determination of the bentonite type and the optimum bentonite-sand mixing ratio is mutually influenced, and should consider the engineering properties and economic requirements.

5. Conclusions

The deformation and saturated permeability behaviour of GCL bentonite-sand mixture under the salt solution infiltration were obtained through the swelling and compression tests. A model for predicting the HM behaviour of bentonite-sand mixtures under the coupled MC effect was proposed subsequently. The following conclusions were drawn:

(1) The e_m-p_e relationship of bentonite-sand mixtures with $\alpha \leq \alpha_s$ saturated by salt solution can be normalized with respect to salt solution and sand content, and presents a linear relationship. When $\alpha > \alpha_s$, the e_m-p_e relationship

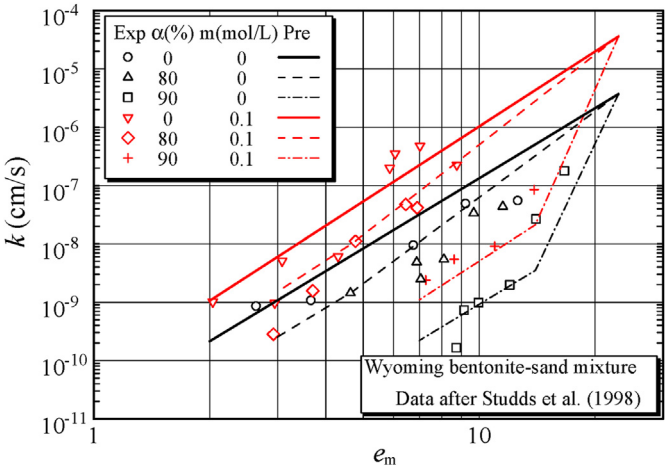

Fig. 24. Permeability prediction of Wyoming bentonite-sand mixtures.

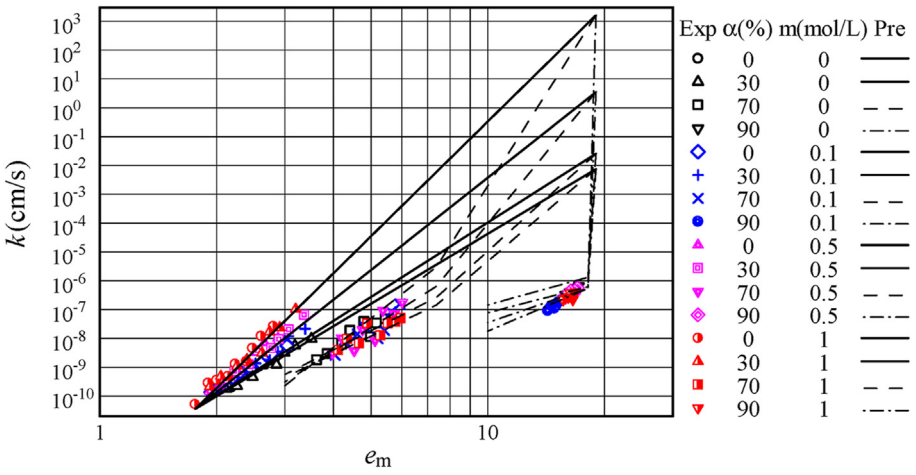

Fig. 25. Permeability prediction of GCL bentonite-sand mixtures.

deviates from the e_m-p_e relation line at the true effective deviatoric stress.

(2) When $\alpha \leq \alpha_s$, the k-e_m relation line of bentonite-sand mixtures saturated by salt solutions with different concentrations intersects at a critical point, and the slope of k-e_m line increases with the increase in salt solution concentration. When $\alpha > \alpha_s$, the k-e_m relationship deviates from the k-e_m line; moreover, the larger the sand content, the farther the deviation. After the deviation, the k-e_m relationship is approximately bi-linear, and the intersection is consistent with the deviation point in the e_m-p_e relationship.

(3) The proposed model can uniformly predict the swelling (including swelling deformation and swelling pressure) and saturated permeability coefficients of different types of bentonite and its sand mixture at a full range of sand content under the salt solution infiltration with different concentrations. Meanwhile, according to the swelling and anti-seepage requirements of the project, the appropriate initial state indices of bentonite-sand mixtures can be quantitatively determined through the model. The proposed model provides the theoretical support for the design and construction of the anti-seepage engineering of bentonite-sand mixtures.

Declaration of competing interest

The authors declare that they have no known competing financial interests or personal relationships that could have appeared to influence the work reported in this paper.

Acknowledgments

The authors are grateful to the National Natural Science Foundation of China (Grant No. 41977214), the National Key R&D Program of China (Grant No. 2019YFC1520500) and the Open Research Fund of State Key Laboratory of Geomechanics and Geotechnical Engineering, Institute of Rock and Soil Mechanics, Chinese Academy of Sciences (Grant No. Z013008) for the financial supports.

References

Alawaji, H.A., 1999. Swell and compressibility characteristics of sand–bentonite mixtures inundated with liquids. J. Appl. Clay Sci. 15 (3/4), 411–430.
ASTM D2435/D2435M-11, 1995. Standard Test Methods for One-Dimensional Consolidation Properties of Soils Using Incremental Loading. ASTM International, West Conshohocken, PA, USA.
AECL, 1994. The Disposal of Canada's Nuclear Fuel Waste: Engineered Barriers Alternatives. AECL-1078COG-93-8. Atomic Energy of Canada Limited (AECL).
Agus, S.S., Schanz, T., 2008. A method for predicting swelling pressure of compacted bentonites. Acta Geotech. 3 (2), 125–137.
Cabalar, A.F., Hasan, R.A., 2013. Compressional behaviour of various size/shape sand–clay mixtures with different pore fluids. Eng. Geol. 164, 36–49.
Castellanos, E., Villar, M.V., Romero, E., Lloret, A., Gens, A., 2008. Chemical impact on the hydro-mechanical behavior of high-density FEBEX bentonite. Phys. Chem. Earth, Parts A/B/C 33, S516–S526.
Cui, S.L., Du, Y.F., Wang, X.P., Huang, S., Xie, W.L., 2018. Influence of temperature on swelling deformation characteristic of compacted GMZ bentonite-sand mixtures. J. Cent. South Univ. (25), 2819–2830.
Evans, J.C., Shackelford, C.D., Yeo, S.S., Henning, J., 2008. Membrane behavior of soil-bentonite slurry-trench cutoff walls. J. Soil Contam. 17 (4), 316–322.
Fan, R.D., Du, Y.J., Reddy, K.R., Liu, S.Y., Yang, Y.L., 2014. Compressibility and hydraulic conductivity of clayey soil mixed with calcium bentonite for slurry wall backfill: initial assessment. Appl. Clay Sci. 101 (2), 119–127.
Gens, A., Alonso, E.E., 1992. A framework for the behaviour of unsaturated expansive clays. Can. Geotech. J. 29 (6), 1013–1032.
Guimaraes, L.D., Gens, A., Sanchez, M., Olivella, S., 2013. A chemo-mechanical constitutive model accounting for cation exchange in expansive clays. Geotechnique 63 (3), 221–234.
Herbert, H.J., Kasbohm, J., Sprenger, H., Fernández, A.M., Reichelt, C., 2008. Swelling pressures of MX-80 bentonite in solutions of different ionic strength. Phys. Chem. Earth, Parts A/B/C 33, S327–S342.
JNC, 1999. H12: Project to Establish the Scientific and Technical Base for HLW Disposal in Japan. Technical Report. Japan Nuclear Cyclic Development Institute (JNC) (in Japanese).
Karnland, O., Nilsson, U., Weber, H., Wersin, P., 2008. Sealing ability of Wyoming bentonite pellets foreseen as buffer material-Laboratory results. Phys. Chem. Earth, Parts A/B/C 33, S472–S475.
Katsumi, T., Ishimori, H., Onikata, M., Fukagawa, R., 2008. Long-term barrier performance of modified bentonite materials against sodium and calcium permeant solutions. Geotext. Geomembranes 26 (1), 14–30.
Komine, H., Ogata, N., 1994. Experimental study on swelling characteristics of compacted bentonite. Can. Geotech. J. 31 (4), 478–490.
Komine, H., 2004. Simplified evaluation on hydraulic conductivities of sand-bentonite mixture backfill. Appl. Clay Sci. 26 (1–4), 13–19.
Komine, H., Ogata, N., 2004. Predicting swelling characteristics of bentonites. J. Geotech. Geoenviron. Eng. 130 (8), 818–829.
Komine, H., 2008. Theoretical equations on hydraulic conductivities of bentonite-based buffer and backfill for underground disposal of radioactive wastes. J. Geotech. Geoenviron. Eng. 134 (4), 497–508.
Komine, H., Yasuhara, K., Murakami, S., 2009. Swelling characteristics of bentonites in artificial seawater. Can. Geotech. J. 46 (2), 177–188.
Ma, T.T., Wei, C.F., Xia, X.L., et al., 2016. Constitutive model of unsaturated soils considering the efect of intergranular physicochemical forces. J. Eng. Mech. 142 (11), 0416088.
Mollins, L.H., Stewart, D.I., Cousens, T.W., 1996. Predicting the properties of bentonite-sand mixtures. Clay Miner. 31 (2), 243–252.
Monkul, M.M., Yamamuro, J.A., 2011. Influence of silt size and content on liquefaction behavior of sands. Can. Geotech. J. 48 (6), 931–942.
Petrov, R.J., Rowe, R.K., Quigley, R.M., 1997. Comparison of laboratory-measured GCL hydraulic conductivity based on three permeameter types. Geotech. Test J. 20 (1), 49–62.
Pacovsky, J., Svoboda, J., Zapletal, L., 2007. Saturation development in the bentonite barrier of the Mock-Up-CZ geotechnical experiment. Phys. Chem. Earth, Parts A/B/C 32 (8), 767–779.

Rao, S., Deepak, G.B., Rao, P.R., Anbazhagan, P., 2017. Influence of physico-chemical components on the consolidation behavior of soft kaolinites. Acta Geotech. 12 (2), 441–451.
Rao, S.N., Mathew, P.K., 1995. Effects of exchangeable cations on hydraulic conductivity of a marine clay. Clay Clay Miner. 43 (4), 433–437.
Sällfors, G., Öberg-Högsta, A.L., 2002. Determination of hydraulic conductivity of sand-bentonite mixtures for engineering purposes. Geotech. Geol. Eng. 20 (1), 65–80.
Shackelford, C.D., Sevick, G.W., Eykholt, G.R., 2010. Hydraulic conductivity of geosynthetic clay liners to tailings impoundment solutions. Geotext. Geomembranes 28 (2), 149–162.
Shirazi, S.M., Kazama, H., Salman, F.A., Othman, F., Akib, S., 2010. Permeability and swelling characteristics of bentonite. Int. J. Phys. Sci. 5 (11), 1647–1659.
Sivapullaiah, P.V., Sridharan, A., Stalin, V.K., 2000. Hydraulic conductivity of bentonite–sand mixtures. Can. Geotech. J. 37 (2), 405–413.
SKB, 2010. Design, Production and Initial State of the Buffer. SKB Technical Report TR-10-15. Swedish Nuclear Fuel and Waste Management Co., Stockholm, Sweden, 2010.
Srikanth, V., Mishra, A.K., 2016. A laboratory study on the geotechnical characteristics of sand–bentonite mixtures and the role of particle size of sand. Int. J. Geosynth. Ground Eng. 2, 3.
Studds, P.G., Stewart, D.I., Cousens, T.W., 1998. The effects of salt solutions on the properties of bentonite-sand mixtures. Clay Miner. 33 (4), 651–660.
Sun, D.A., Cui, H.B., Sun, W.J., 2009. Swelling of compacted sand-bentonite mixtures. Appl. Clay Sci. 43 (3), 485–492.
Sun, W.J., Sun, D.A., 2016. Response to "Discussion on "Evaluation of the swelling characteristics of bentonite-sand mixtures". Eng. Geol. 209, 211–214.
Sun, D.A., Zhang, J.Y., Zhang, J.R., Zhang, L., 2013. Swelling characteristics of GMZ bentonite and its mixtures with sand. Appl. Clay Sci. 83, 224–230.
Sun, W.J., Liu, S.Q., Sun, D.A., Fang, L., 2014. Swelling characteristics and permeability of bentonite. In: Proceedings of the 6th International Conference on Unsaturated Soils, pp. 1211–1217.
Sun, D.A., Zhang, L., Li, J., Zhang, B.C., 2015a. Evaluation and prediction of the swelling pressures of GMZ bentonites saturated with saline solution. J. Appl. Clay Sci. 105–106, 207–216.
Sun, W.J., Wei, Z.F., Sun, D.A., Liu, S.Q., Fatahi, B., Wang, X.Q., 2015b. Evaluation of the swelling characteristics of bentonite-sand mixtures. J. Eng. Geol. 199, 1–11.
Sun, W.J., Zong, F.Y., Sun, D.A., Schanz, T., Behzad, F., 2017. Swelling prediction of bentonite-sand mixtures in the full range of sand content. J. Eng. Geol. 222, 146–155.
Thevanayagam, S., Nesarajah, S., 1998. Fractal model for flow through saturated soils. J. Geotech. Geoenviron. Eng. 124 (1), 53–66.
Tripathi, K., 2013. Hydraulic conductivity prediction of saturated sand-bentonite mixtures. Geotech. Geol. Eng. 31 (2), 581–591.
Villar, M.V., Lloret, A., 2008. Influence of dry density and water content on the swelling of a compacted bentonite. Appl. Clay Sci. 39 (1–2), 38–49.
Wang, D.W., Zhu, C., Tang, C.S., Li, S.J., Cheng, Q., Pan, X.H., Shi, B., 2021. Effect of sand grain size and boundary condition on the swelling behavior of bentonite–sand mixtures. Acta Geotech. 16, 2759–2773.
Wang, Q., Tang, A.M., Cui, Y.J., Delage, P., Gatmiri, B., 2012. Experimental study on the swelling behavior bentonite/claystone mixture. Eng. Geol. 124, 59–66.
Wang, J., 2010. High-level radioactive waste disposal in China: update 2010. J. Rock Mech. Geotech. Eng. 2 (1), 1–11.
Wang, J., Chen, L., Su, R., Zhao, X.G., 2018. The Beishan underground research laboratory for geological disposal of high-level radioactive waste in China: planning, site selection, site characterization and in situ tests. J. Rock Mech. Geotech. Eng. 10 (3), 411–435.
Wei, C.F., 2014. A theoretical framework for modeling the chemomechanical behavior of unsaturated soils. Vadose Zone J. 13 (9), 1–21.
Xu, Y., Xiang, G., Jiang, H., Chen, T., Chu, F.F., 2014. Role of osmotic suction in volume change of clays in salt solution. Appl. Clay Sci. 101, 354–361.
Ye, W.M., Chen, Y.G., Chen, B., Wang, Q., Wang, J., 2010. Advances on the knowledge of the buffer/backfill properties of heavily-compacted GMZ bentonite. Eng. Geol. 116, 12–20.
Ye, W.M., Zhang, F., Chen, B., Chen, Y.G., Wang, Q., Cui, Y.J., 2014. Effects of salt solutions on the hydro-mechanical behavior of compacted GMZ01 Bentonite. Environ. Earth Sci. 72 (7), 2621–2630.
Zhang, H.Y., Cui, S.L., Zhang, M., Jia, L.Y., 2012a. Swelling behaviors of GMZ bentonite–sand mixtures inundated in NaCl-Na_2SO_4 solutions. Nucl. Eng. Des. 242, 115–123.
Zhang, M., Zhang, H.Y., Cui, S.L., Jia, L.Y., Zhou, L., Chen, H., 2012b. Engineering properties of GMZ bentonite-sand as buffer/backfilling material for high-level waste disposal. Eur. J. Environ. Civ. Eng. 16 (10), 1216–1237.
Zhu, C.M., Ye, W.M., Chen, Y.G., Chen, B., Cui, Y.J., 2013. Influence of salt solutions on the swelling pressure and hydraulic conductivity of compacted GMZ01 bentonite. Eng. Geol. 166, 74–80.

Wenjing Sun obtained her BSc degree in Civil Engineering from Qingdao University of Technology, China, in 2002, her MSc degree in Structural Engineering from Shanghai University, China, in 2005 and her PhD in Unsaturated Soil Mechanics in 2009, also from Shanghai University. She is a Professor and PhD supervisor at Donghua University. Her research interests cover unsaturated soil mechanics, laboratory testing, constitutive modeling, environmental geotechnics, nuclear waste disposal, solid waste resource utilization, etc. She has published more than 70 scientific papers. She has published a book "*Experimental Technique in Unsaturated Soil Mechanics*". She has won the first prize of Natural Science of Ministry of Education in China (ranking the 4th) and the Outstanding Achievement of Graduate Student in Shanghai (Doctoral Dissertation).